IMMUNOLOGY

Remodeling of metabolism and inflammation by exercise ameliorates tumor-associated anemia

Regula Furrer[1], Annaïse J. Jauch[2], Tata Nageswara Rao[3†‡], Sedat Dilbaz[1], Peter Rhein[4], Stefan A. Steurer[1], Mike Recher[2], Radek C. Skoda[3], Christoph Handschin[1]*

A considerable number of patients with cancer suffer from anemia, which has detrimental effects on quality of life and survival. The mechanisms underlying tumor-associated anemia are multifactorial and poorly understood. Therefore, we aimed at systematically assessing the patho-etiology of tumor-associated anemia in mice. We demonstrate that reduced red blood cell (RBC) survival rather than altered erythropoiesis is driving the development of anemia. The tumor-induced inflammatory and metabolic remodeling affect RBC integrity and augment splenic phagocyte activity promoting erythrophagocytosis. Exercise training normalizes these tumor-associated abnormal metabolic profiles and inflammation and thereby ameliorates anemia, in part, by promoting RBC survival. Fatigue was prevented in exercising tumor-bearing mice. Thus, exercise has the unique potential to substantially modulate metabolism and inflammation and thereby counteracts pathological remodeling of these parameters by the tumor microenvironment. Translation of this finding to patients with cancer could have a major impact on quality of life and potentially survival.

INTRODUCTION

Cancer is the second leading cause of death worldwide and, according to the World Health Organization, is responsible for nearly 10 million deaths per year. Besides cachexia, anemia is one of the most frequently reported complications of cancer. Approximately one-third of newly diagnosed patients with cancer suffer from anemia before any treatment (*1*, *2*). Most of these patients have mild anemia, but even such low pretreatment hemoglobin (Hb) levels are associated with reduced survival (*2*, *3*). Moreover, in response to tumor-reductive therapy, 75% of patients will develop anemia (*1*). Cancer-related anemia is associated with fatigue and a substantial reduction in quality of life (*4*, *5*) and is an independent predictor for survival (*6*). The current standard care for anemic patients with cancer exclusively focuses on augmenting erythropoiesis and is limited to iron supplementation, erythropoiesis-stimulating agents such as erythropoietin (EPO), or blood transfusion for patients suffering from severe anemia (*7*). However, treating cancer patients with recombinant EPO remains controversial as malignant cells express EPO receptors, and the treatment is even associated with increased mortality (*8*, *9*). Notably, however, the causes of cancer-related anemia are multifactorial and can include blood loss, reduced intake or absorbance of nutrients, and suppression of hematopoiesis by malignant bone marrow infiltration or radio-/chemotherapy (*10*). Furthermore, systemic effects of cancer, such as elevated cytokines levels, could also promote the development of anemia synergizing with direct consequences of tumor load or treatment modalities (*7*). Accordingly, plasma levels of the proinflammatory cytokines interleukin-1β (IL-1β), IL-6, and tumor necrosis factor–α (TNFα) are negatively correlated with Hb levels in patients with cancer (*11*). In addition to patients with cancer, anemia is often observed in patients with chronic inflammatory diseases such as congestive heart failure or chronic pulmonary or kidney diseases (*7*). The inflammatory environment might promote anemia in a pleiotropic manner, although causality is ill-defined. For example, compared to patients suffering from iron deficiency anemia without malignancy who have highly elevated EPO levels, in anemic patients with cancer, EPO production is blunted (*12*). This is potentially mediated by circulating cytokines, with likely implications on erythropoiesis (*13*). Red blood cell (RBC) production could further be dysregulated by impaired iron utilization because of IL-6–stimulated hepcidin production in the liver, thereby reducing iron availability for erythropoiesis (*14*). Curiously, however, administration of very high doses of IL-6 (i.e., 1 mg/kg) boosts medullary and extramedullary erythropoiesis (*15*). In contrast, injecting high doses of IL-1 or TNFα suppresses maturation of erythroid progenitors (*16*, *17*). Thus, although an association between inflammation and the production of RBCs has been postulated, most studies are correlative or used high doses of the candidate cytokines.

In addition to the impaired production, RBC survival is also reduced in patients with conditions associated with high levels of inflammation such as rheumatoid arthritis or chronic diseases (*18*, *19*). This suggests that proinflammatory cytokines could also reduce RBC half-life (*20*). RBC life span in tumor-bearing (TB) mice seems to be decreased because of elevated apoptosis of erythrocytes, so-called eryptosis (*21*), which also has been reported in anemic patients with cancer (*22*). However, most assumptions are based on correlations, and it remains elusive which factors alter RBC survival and could thereby be involved in the development of tumor-associated anemia. Notably, in addition to cytokines, many other substances (i.e., oxysterols and reactive oxygen species) and stressors (i.e., glucose starvation) inducing distinct metabolic responses in RBCs have been shown to promote eryptosis (*23*–*26*). It is conceivable that the tumor-induced systemic remodeling alters the RBC niche that is crucial for its survival. Hence, the

[1]Biozentrum, University of Basel, Basel, Switzerland. [2]Immunodeficiency Laboratory, Department of Biomedicine, University Hospital Basel and University of Basel, Basel, Switzerland. [3]Experimental Hematology, Department of Biomedicine, University Hospital Basel and University of Basel, Basel, Switzerland. [4]Luminex B.V., 's-Hertogenbosch, Netherlands.
*Corresponding author. Email: christoph.handschin@unibas.ch
†Present address: Department of Hematology and Central Hematology Laboratory, Inselspital, Bern University Hospital, University of Bern, Bern, Switzerland.
‡Present address: Department for BioMedical Research, University of Bern, Bern, Switzerland.

underlying mechanisms of tumor-associated anemia are still poorly understood.

In summary, despite the large number of patients with cancer suffering from anemia and the marked detrimental effects of anemia on quality of life and survival, there is still a lack of knowledge on the pathophysiology of tumor-associated anemia, leading to an insufficient portfolio of treatment avenues. Consequently, it is instrumental to obtain a better understanding of the mechanistic aspects related to RBC production, maturation, and elimination in this disease context. Because of the limited possibilities to analyze the different facets of anemia in patients with cancer, we used a mouse tumor model that develops robust anemia and recapitulates pathological key features observed in patients with cancer (*27*). This allows a thorough dissection of the effects of tumor growth on different organs and on systemic remodeling. Our study revealed that tumor-associated anemia was mainly caused by reduced RBC survival, without impairments in erythropoiesis. We provide solid evidence that the tumor-induced metabolic and immune dysregulation accentuated RBC fragility and made them more susceptible for phagocyte-mediated elimination. We lastly used exercise as a potential intervention, since training-based therapies are currently being tested to mitigate cachexia, the other most common cancer complication besides anemia. Therapeutically, we demonstrate that endurance training markedly normalized the RBC environment, thereby attenuated the development of anemia and improved performance, all of which could have meaningful implications for the treatment of patients with cancer.

RESULTS

Tumors lead to reduced RBC survival rather than impaired erythropoiesis

To investigate the systemic alterations responsible for the anemia caused by the tumor rather than metastasis, blood loss, or chemotherapy, we used a well-established primary cancer model and injected Lewis lung cancer (LLC) cells subcutaneously into the flank of C57BL/6J mice. LLC tumors (weighing 1005 ± 284 mg after 3.5 weeks; $n = 6$) induce severe anemia within 3.5 weeks, reaching Hb levels below 5 g/dl (Fig. 1A). To analyze whether this substantial drop in Hb was caused by reduced erythropoiesis, $Ter119^+$ erythroid cells were assessed in bone marrow and the spleen. In stark contrast to the remarkable anemia in the periphery, erythropoiesis was not impaired in TB mice but was even increased as reflected by the higher percentage of $Ter119^+$ cells in the spleen (Fig. 1B). This erythropoietic potential of the spleen in TB mice is also demonstrated by the threefold elevation in the relative number of $CD71^+$ erythroid precursors and the massive induction of mRNA expression of genes involved in erythropoiesis and heme synthesis (Fig. 1C). Gene expression was measured in whole-tissue homogenate of the spleen and therefore includes changes in the cell population of the spleen. In line with these results, we observed a relative augmentation of the premature stages II, III, and IV in $Ter119^+$ bone marrow and spleen cells in TB compared to healthy control (Ctrl) mice, whereas fully mature stage V RBCs were relatively reduced (Fig. 1, D and E). This suggests that there is an accelerated release of premature RBCs to meet the elevated demand. Accordingly, there was a higher percentage of premature stage IV and a decrease in stage V RBCs in the blood of TB as compared to Ctrl animals (Fig. 1F). These observations were further substantiated by assessing the abundance of CD71 and DNA content by DRAQ5 in $Ter119^+$ cells (fig. S1). Similar to the $CD44^+$ cells, the relative amount of $CD71^+Ter119^+$ cells was considerably elevated, indicating a higher number of premature RBCs in TB mice (fig. S1A). The absence of DRAQ5 in these $CD71^+Ter119^+$ cells suggests that these are reticulocytes and already expelled their nucleus (fig. S1B). These findings are also reflected in the larger RBCs of TB mice (Fig. 1G). Together, these data imply that rather than impaired, erythropoiesis is massively increased in TB mice and does therefore not provide an adequate explanation for the observed anemia.

Next, we tested whether the removal of RBCs is elevated in TB animals and could contribute to the severe reduction in Hb. To measure RBC removal/survival, mice were injected with sulfo–*N*-hydroxysuccinimide (NHS)–Biotin intravenously before tumor initiation and biotinylated $Ter119^+$ RBCs were analyzed longitudinally in peripheral blood. Mirroring anemia, RBC elimination was accelerated in TB mice throughout tumor development (Fig. 2A). Thus, to investigate whether RBCs of TB mice are more stressed and show abnormalities, we assessed phosphatidylserine externalization, a cellular marker of enhanced eryptosis. In TB mice, a fivefold increase in the number of phosphatidylserine-exposing RBCs was found as measured by annexin V binding (Fig. 2B), implying an inherent predisposition for phagocytosis. As the spleen is the main organ for RBC removal (*28*), the massive splenomegaly in TB mice (Fig. 2C) could be instrumental for the compromised RBC survival. To gain insight into the origin of this splenomegaly, we assessed the cell composition of spleens of Ctrl and TB mice. Notably, the number of $CD45^+$ cells was markedly reduced to approximately one-third of that of a Ctrl spleen (Fig. 2D). However, when calculating the total number of $CD45^+$ cells per spleen, this difference disappeared when taking into account the spleen mass and number of cells, indicating that the enlargement of the spleen is not caused by leukocyte expansion. Within the $CD45^+$ population, lymphoid cell numbers were similar between Ctrl and TB mice, with only a slight reduction in the relative amount of T cells in TB animals (Fig. 2E). The main changes occurred in myeloid cells, which were more abundant because of a relative increase in $F4/80^{high}$ macrophages and $CD11b^{high}$ monocytes/neutrophils in TB compared to Ctrl mice. Of the $CD45^-$ splenocytes, more than 50% were $CD71^+$ in TB mice, while in a healthy spleen, less than 10% of splenocytes are $CD71^+$ (Fig. 2F). Our data demonstrate that the splenomegaly in TB mice is not the result of leukocyte expansion but rather the consequence of increased extramedullary erythropoiesis reflected by the high number of $CD71^+$ erythroid precursors and the elevated transcription of genes involved in erythropoiesis (Fig. 1C).

To investigate whether splenic RBC elimination is enhanced in TB mice, we performed an in vitro erythrophagocytosis assay. Splenocytes were isolated from Ctrl and TB animals and coincubated with PKH26 fluorescently labeled healthy Ctrl RBCs. After 1 hour, RBCs were lysed and splenocytes were analyzed by flow cytometry. Next, we used ImageStream® to visualize $PKH26^+$ phagocytes. The gates were set according to the fluorescence of the PKH26-labeled RBC (Fig. 3, A and B). More specifically, $PKH26^{med}$ phagocytes showed the same intensity as PKH26-labeled RBC, while $PKH26^{high}$ phagocytes have a higher fluorescent signal. First, we determined whether the RBCs were internalized by the phagocytes by determining the internalization score and observed that only $PKH26^{high}$ phagocytes showed complete internalization of the RBCs with a score above 0 (Fig. 3C and fig. S2A). The images of the different populations also

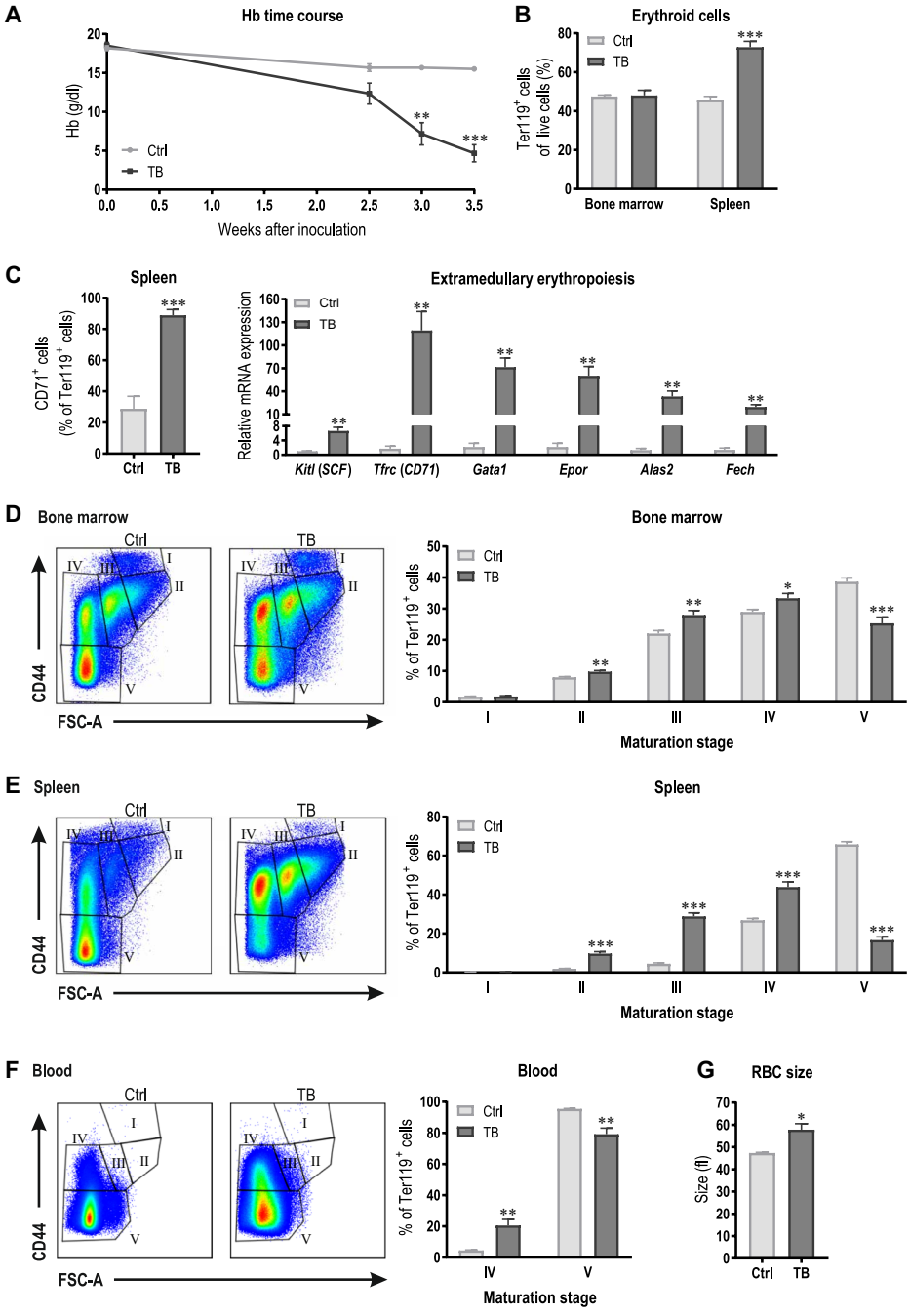

Fig. 1. Tumor-associated anemia is accompanied by augmentation of extramedullary erythropoiesis. Tumor was induced by injecting LLC cells into the flank of mice. (**A**) Time course of Hb levels in Ctrl and TB mice throughout the study. (**B**) Ter119$^+$ erythroid cells were assessed in the bone marrow and spleen by flow cytometry. (**C**) CD71$^+$ cells within the Ter119$^+$ population were determined, and mRNA levels of gene involved in erythropoiesis and heme synthesis were measured in whole-spleen homogenate by semi quantitative polymerase chain reaction (qPCR). (**D** to **F**) Maturation of Ter119$^+$ cells were analyzed according to their size and CD44 expression in the bone marrow (D), spleen (E), and blood (F) as shown in the representative flow cytometry plots and quantified in the bar graphs. (**G**) RBC size was assessed during the blood count using Advia 2021 (mean corpuscular volume). Groups ($n = 6$ per group) were compared by two-tailed unpaired *t* tests with Welch's correction, and data are represented as means + SEM. Asterisks indicate differences between Ctrl and TB group. $^*P < 0.05$, $^{**}P < 0.01$, and $^{***}P < 0.001$. Kilt/SCF, kit ligand/stem cell factor; Tfrc/CD71, transferrin receptor; Gata1, GATA binding protein (erythroid transcription factor); Epor, EPO receptor; Alas2, 5′-aminolevulinate synthase 2 (erythroid-specific); Fech, ferrochelatase; FSC-A, forward scatter area.

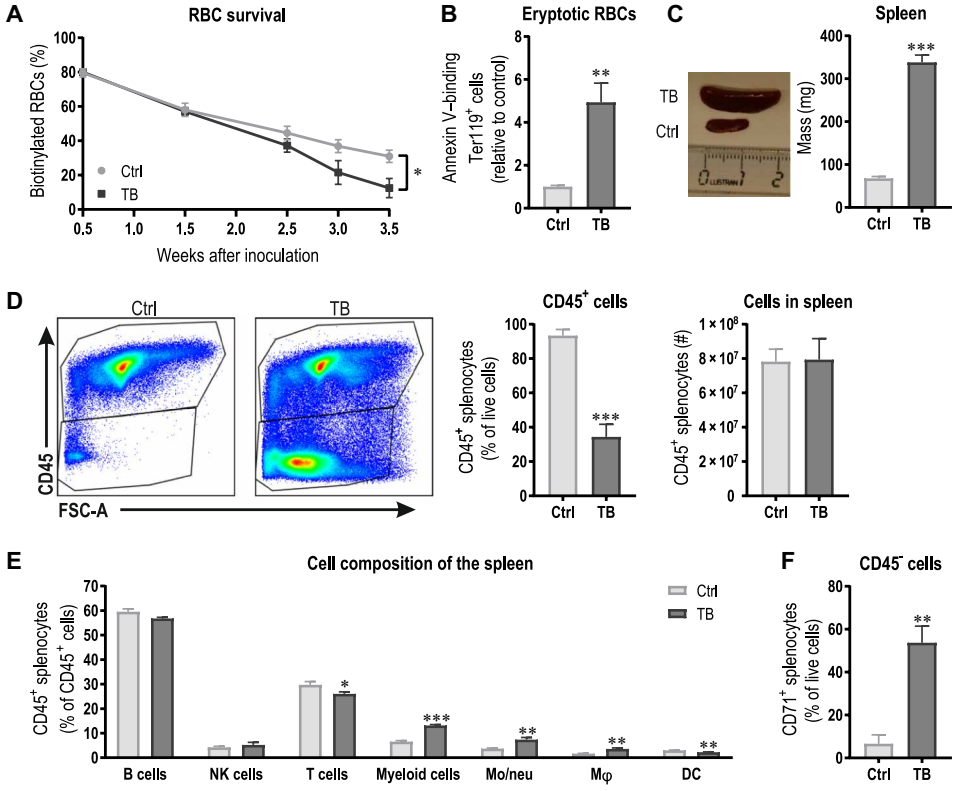

Fig. 2. Cancer-related anemia is caused by reduced RBC survival. (**A**) RBC survival of Ctrl and TB mice was assessed by measuring biotinylated Ter119$^+$ RBCs throughout the study. (**B**) As a measure for RBC eryptosis propensity and susceptibility for erythrophagocytosis, phosphatidylserine externalization in Ter119$^+$ RBCs was assessed by annexin V binding. (**C**) Representative picture and spleen mass quantification of Ctrl and TB mice 3.5 weeks after tumor cell inoculation. The ruler is in centimeters. (**D**) Representative flow cytometry plots of viable splenocytes and relative and absolute quantification of CD45$^+$ cells taking into account the spleen mass and cell number. (**E**) Spleen cell composition with regard to leukocytes was analyzed by flow cytometry. NK, natural killer; DC, dendritic cell. (**F**) CD45$^-$CD71$^+$ cells were assessed. Groups ($n = 5$ to 6 per group) were compared by two-tailed unpaired *t* tests with Welch's correction and data are represented as means + SEM. Asterisks indicate differences between Ctrl and TB group. *$P < 0.05$, **$P < 0.01$, and ***$P < 0.001$. Photo credit: Regula Furrer, University of Basel.

revealed that PKH26^{med} phagocytes predominantly contain PKH26$^+$ fragments (Fig. 3D and fig. S2B), which could be the result of small vesicles originating form phosphatidylserine-positive RBCs (*29*). In contrast to the fragments observed in PKH26^{med} phagocytes, PKH26^{high} phagocytes engulfed the entire RBCs (Fig. 3D and fig. S2B). Therefore, we determined the relative amount of PKH26^{high} F4/80^{high}CD11b^{low} red pulp macrophages (RPMs), F4/80^{high}CD11b^{high} macrophages, and F4/80^{low}CD11b^{high} monocytes/neutrophils (Fig. 3, E to G). Notably, the percentage of highly fluorescent F4/80^{high}CD11b^{low} RPMs and F4/80^{high}CD11b^{high} macrophages were elevated in TB compared to Ctrl mice (Fig. 3, F and G). Considering the higher abundance of macrophages in TB mice combined with the boosted phagocytic activity of these macrophages to remove RBCs, we provide evidence for the tremendous potential of the spleen of TB mice for erythrophagocytosis.

Together, our results reveal that splenic macrophages of TB mice are more activated and phagocytose a higher number of healthy RBCs. Subsequently, we were interested whether RBCs of TB animals are also more susceptible to be removed by macrophages. To test this, we cocultured splenocytes of healthy Ctrl mice with PKH26-labeled RBCs from Ctrl versus TB animals. A particular cell population showed enhanced removal of RBCs from TB mice. More specifically, a higher percentage of F4/80^{low}CD11b^{high} monocytes/neutrophils were PKH26^{high} (Fig. 3, H and I), which is in line with previous reports showing that neutrophils specifically increase erythrophagocytosis of stressed RBCs (*30*). We made an intriguing observation regarding differences in RBC morphology between Ctrl and TB mice (fig. S2, C and D). A larger proportion of RBCs of TB mice showed a stomatocyte-like morphology, while the population displaying healthy discocyte-like morphology was reduced. This RBC abnormality is also seen in RBCs of long-stored blood and is linked to an elevated susceptibility for phagocyte-mediated removal (*31*). In summary, splenic macrophages are activated in TB animals and show an elevated activation to remove RBCs from the circulation. In addition, RBCs of TB mice show abnormalities reflected by the increased phosphatidylserine exposure and altered morphology and are therefore more susceptible to be eliminated by phagocytes. Collectively, these tumor-induced alterations result in a reduced RBC survival, which subsequently contributes to the development of tumor-associated anemia.

An altered metabolic and immune profile negatively affects RBC survival

To investigate how the tumor contributes to RBC abnormalities such as phosphatidylserine externalization, systemic factors that could affect the RBC niche were assessed. The cytokines TNFα and IL-1β that are suggested to reduce RBC survival were measured in plasma of Ctrl and TB mice. At this time point, only IL-1β was elevated in

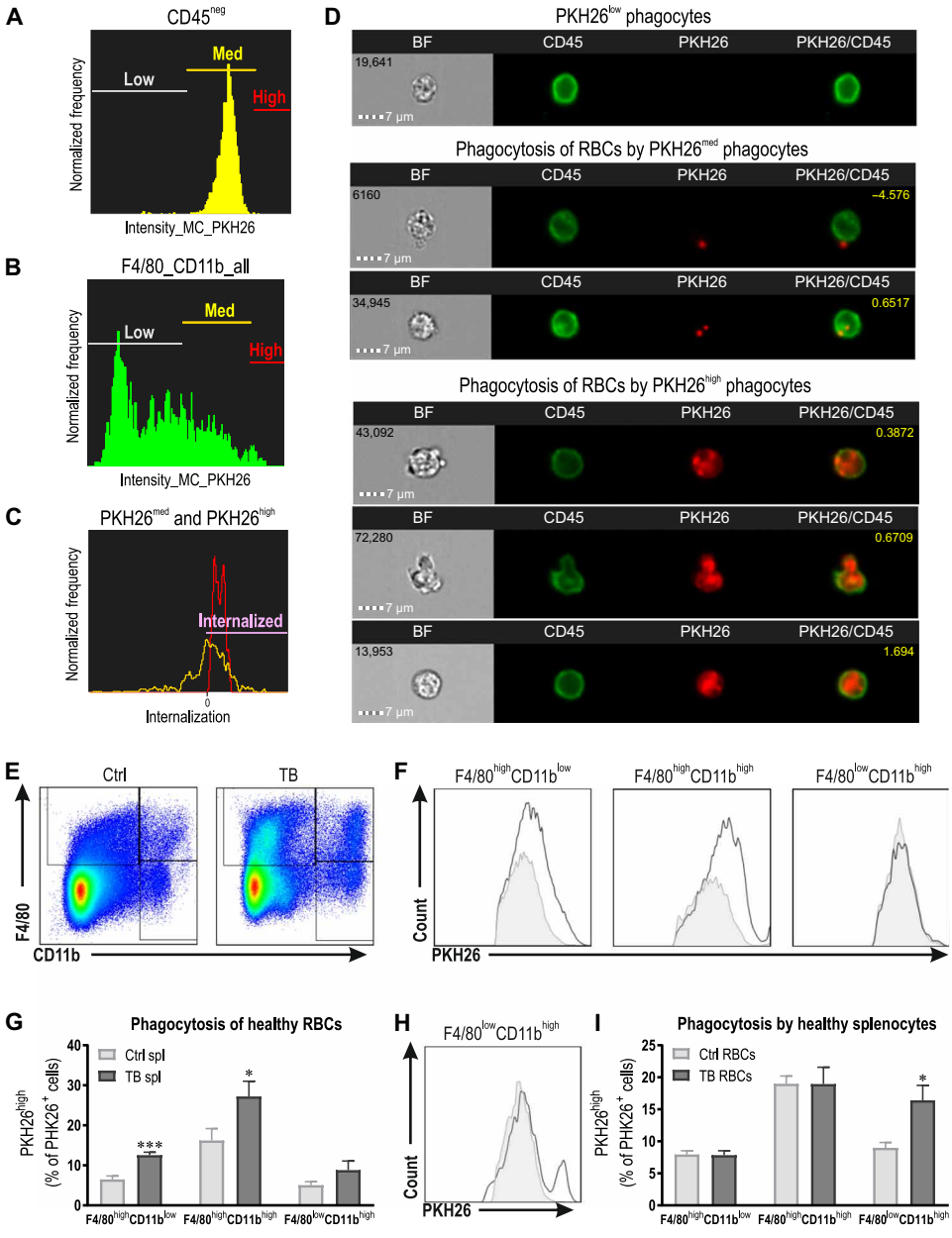

Fig. 3. Erythrophagocytosis is substantially elevated in TB mice. (**A** to **D**) Validation of the erythrophagocytosis assay using ImageStream®. Gates for PKH26^{low}, PKH26^{med}, and PKH26^{high} were set according to the fluorescence of the PKH26-labeled RBCs (A), and phagocytes were analyzed accordingly (B). The rate of internalization of PKH26^{med} (yellow) and PKH26^{high} (red) cells was determined (a score higher than 0 is considered internalized), and the three different populations were visualized (D). Only PKH26^{high} phagocytes show complete internalization and engulfment of entire RBCs. These plots and images are from the erythrophagocytosis experiment in which RBCs from TB mice were coincubated with healthy Ctrl splenocytes. (**E**) Representative flow cytometry plots with the gating strategy for F4/80^{high}CD11b^{low} red pulp macrophages, F4/80^{high}CD11b^{high} macrophages, and F4/80^{low}CD11b^{high} monocytes/neutrophils (gated on CD45^{+} splenocytes). (**F** and **G**) PKH26 fluorescently labeled healthy RBCs were coincubated with splenocytes (spl) of either Ctrl or TB mice. Representative histograms of PKH26^{+} phagocytes including PKH26^{med} and PKH26^{high} (F) and the quantification of the percentage PKH26^{high} cells representing phagocytes that engulfed complete RBCs (G). (**H** and **I**) PKH26 fluorescently labeled RBCs from Ctrl or TB mice were coincubated with healthy splenocytes. Representative histogram of PKH26^{+} F4/80^{low}CD11b^{high} monocytes/neutrophils (H) and the quantification of the percentage PKH26^{high} cells representing phagocytes that engulfed complete RBCs (I). Groups ($n = 5$ to 6 per group) were compared by two-tailed unpaired *t* tests with Welch's correction and data are represented as means + SEM. Asterisks indicate differences between Ctrl and TB group. *$P < 0.05$ and ***$P < 0.001$.

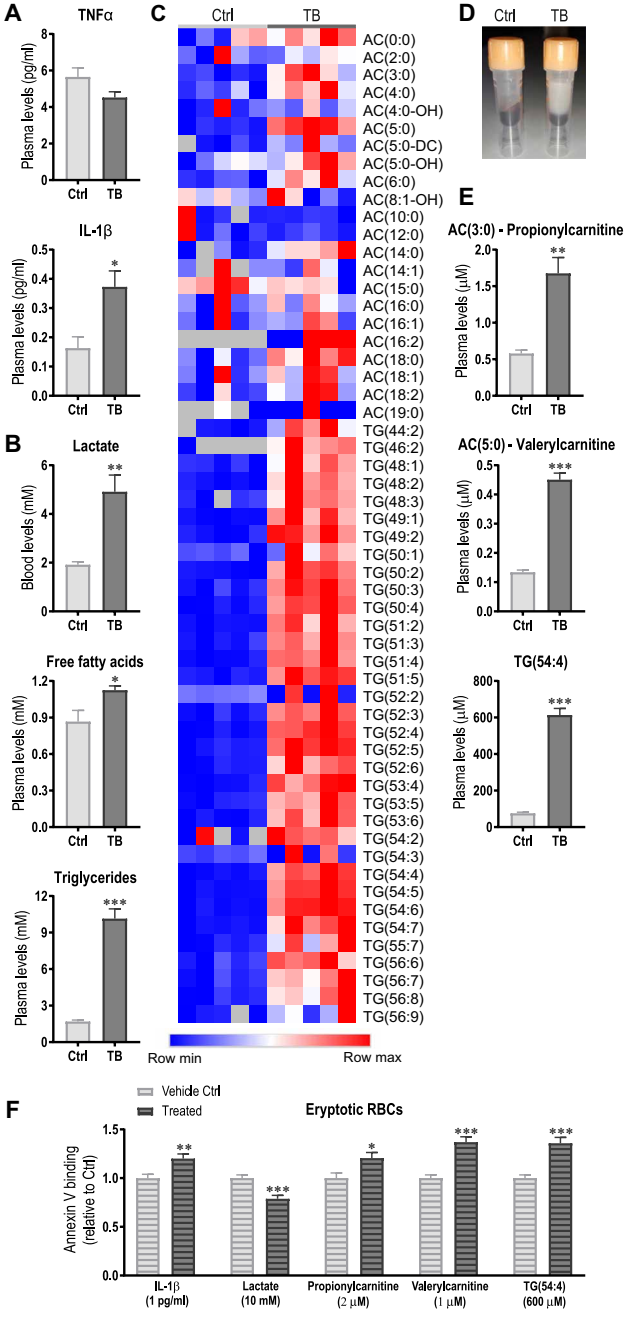

Fig. 4. Tumor-induced metabolic remodeling and immune activation promotes eryptosis. (**A** and **B**) Levels of proinflammatory cytokines TNFα and IL-1β (A) and blood lactate, free fatty acids, and triglycerides (B) were analyzed in plasma of Ctrl and TB mice 3.5 weeks after tumor inoculation. (**C**) Heatmap of acylcarnitines (ACs) and triglycerides (TGs) from the metabolomics analysis. (**D**) Representative picture of plasma of Ctrl and TB mice demonstrating the massive elevation of lipids. (**E** and **F**) The effects of candidates identified in metabolomics analysis (E) and IL-1β and lactate on eryptosis were tested by incubating healthy RBCs with the observed levels of IL-1β or the different metabolites. After 24 hours, eryptosis was measured by assessing phosphatidylserine externalization via annexin V binding using flow cytometry (F). Groups ($n = 5$ to 7 per group) were compared by two-tailed unpaired *t* tests with Welch's correction and data are represented as means + SEM. Data of in vitro eryptosis experiments consist of three independent experiments with three to four biological replicates. Asterisks indicate differences between Ctrl and TB/treated group. $^{*}P < 0.05$, $^{**}P < 0.01$, and $^{***}P < 0.001$. Photo credit: Regula Furrer, University of Basel.

plasma of TB mice compared to Ctrl (Fig. 4A). Since the tumor induces major metabolic remodeling that could alter RBC environment, blood lactate levels and plasma levels of free fatty acids and triglycerides were determined and were shown to be substantially elevated (Fig. 4B). To obtain a global and unbiased overview of factors potentially promoting eryptosis, mass spectrometry–based metabolomics of the plasma was performed. This metabolomics analysis revealed a remarkable increase in many of the measured acylcarnitines and triglycerides in TB compared to Ctrl mice, visibly reflected in the opaque color of the plasma (Fig. 4, C to E). To test whether IL-1β or any of the metabolites could induce eryptosis, RBCs were isolated from healthy mice and treated with the identified candidates using concentrations similar to those measured in TB mice for 24 hours. Subsequently, eryptotic phosphatidylserine–exposing RBCs were assessed by annexin V binding (Fig. 4F). Notably, the tested triglycerides and acylcarnitines are only a selection of the large number of lipid species that was changed, and the candidates were selected on the basis of their abundance in Ctrl and TB mice. Lactate treatment reduced phosphatidylserine externalization as compared to vehicle treatment, suggesting that lactate is not likely to induce the eryptosis observed in vivo. In contrast, IL-1β, the two acylcarnitines propionylcarnitine [AC(3:0)] and valerylcarnitine [AC(5:0)] as well as TG(54:4) increased phosphatidylserine externalization (Fig. 4F). Mechanistically, we could show that IL-1 receptor 1 (IL1R1) is expressed on RBC and that IL-1β may promote phosphatidylserine externalization by activating caspase 3 (fig. S3) (*32*). Our data thus demonstrate that these metabolites and IL-1β promote eryptosis and might thereby contribute to the reduced RBC survival observed in TB mice.

The altered lipid profile in TB mice is caused by increased lipolysis in adipose tissue and reduced fatty acid oxidation in the liver

To shed light on the causes of the altered metabolic profile, we assessed body composition of Ctrl and TB mice using EchoMRI. In agreement with frequently reported cachexia during tumor development (*33*), fat mass was substantially reduced in TB mice (Fig. 5A). More specifically, epididymal and subcutaneous white adipose tissue (eWAT and sWAT, respectively) was considerably lower in TB mice (Fig. 5B). To test whether the tumor provoked metabolic remodeling in the liver in addition to elevated lipolysis in adipose tissue, expression levels of genes involved in fatty acid uptake and oxidation were assessed in hepatic tissue. Fatty acid uptake into the cytosol does not seem to be altered, as expression of the fatty acid transporters *CD36* was unchanged (Fig. 5C). In contrast, expression levels of carnitine palmitoyltransferase 1a (*Cpt1a*) and *Cpt2* were lower in TB mice, suggesting that fatty acid uptake into the mitochondria is diminished. In addition to the reduced mitochondrial uptake, mRNA expression of genes involved in fatty acid oxidation and oxidative metabolism was also decreased in TB mice (Fig. 5C). Our findings suggest that the reduced oxidative metabolism and fatty acid oxidation in the liver could contribute to the accumulation of acylcarnitines and triglycerides in plasma of TB mice and thereby affect RBC environment.

Exercise ameliorates tumor-associated anemia

As tumor-induced metabolic remodeling leading to substantial elevation of acylcarnitines and triglycerides potentially contributes to the reduced RBC survival and thereby anemia, we investigated

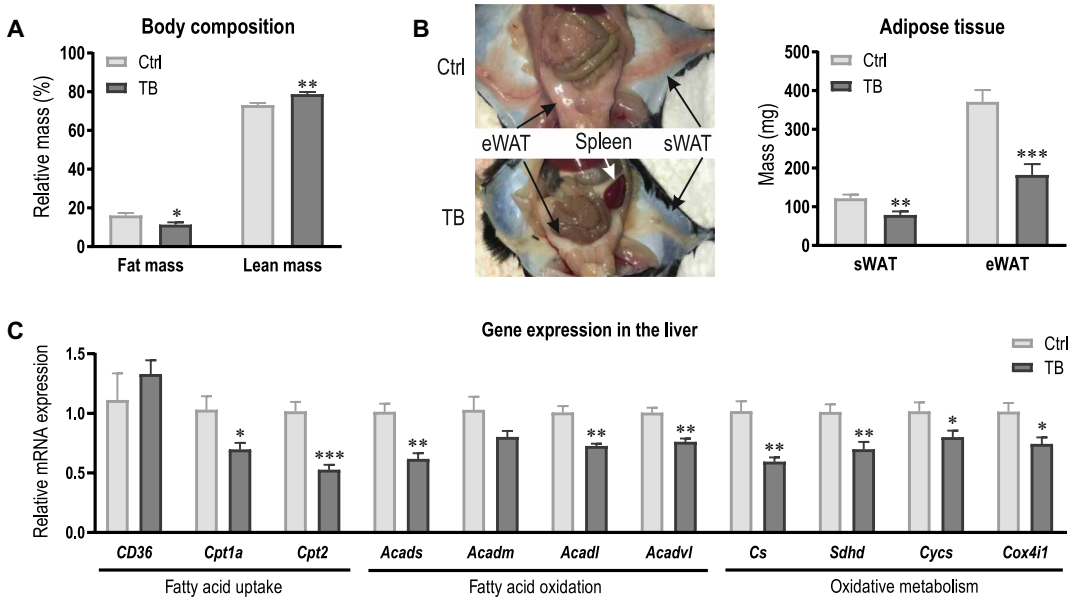

Fig. 5. Increased lipolysis and reduced fatty acid oxidation in the liver contributes to altered lipid profile in TB mice. (**A**) Body composition of Ctrl and TB mice assessed by EchoMRI at the end of the study. (**B**) Representative image depicting the fat loss and splenomegaly in TB mice. Quantification of eWAT and sWAT mass. (**C**) Relative mRNA expression levels of genes involved in fatty acid uptake and oxidation and oxidative capacity were measured in the liver of Ctrl and TB mice. Groups ($n = 6$ to 7 per group) were compared by two-tailed unpaired t tests with Welch's correction and data are represented as means + SEM. Asterisks indicate differences between Ctrl and TB group. $^*P < 0.05$, $^{**}P < 0.01$, and $^{***}P < 0.001$. Cpt, Carnitine palmitoyltransferase; Acad, acyl-CoA dehydrogenases; Cs, citrate synthase; Sdh, succinate dehydrogenase; Cycs, cytochrome c; Cox, cytochrome c oxidase. Photo credit: Regula Furrer, University of Basel.

whether normalizing the lipid profile by pharmacological or physiological interventions could ameliorate the development of anemia. To address this question, we aimed at reducing plasma triglyceride levels by increasing fatty acid oxidation in the muscle or liver pharmacologically by treating mice with peroxisome proliferator–activated receptor β/δ (PPARδ) (GW501516) or PPARα (fenofibrate) agonists, respectively, or physiologically by endurance exercise. While the pharmacological interventions primarily target lipid metabolism, exercise obviously is multifactorial, with systemic benefits, including anti-inflammatory effects. The different interventions did not affect tumor growth, and tumor mass was similar between TB mice and TB mice treated with either PPARδ or PPARα agonists or TB mice that performed exercise (fig. S4). Only TB mice and mice of the pharmacological intervention groups lost fat mass (Fig. 6A). Despite the elevated lipolysis, increasing fatty acid oxidation in the liver by the PPARα agonist fenofibrate substantially lowered triglyceride levels, which was not observed after the treatment with the PPARδ agonist GW501516 (Fig. 6B). This suggests that enhancing fatty acid oxidation in the muscle alone was not sufficient to reduce triglyceride levels. Notably, the metabolic remodeling by exercise, including an increase in fatty acid oxidation, significantly lowered triglyceride levels compared to TB mice (Fig. 6B). To determine whether the normalization of the lipid profile could ameliorate RBC survival, eryptosis of RBCs was assessed. In fenofibrate- and GW501516-treated TB mice, annexin V binding was not elevated compared to Ctrl mice (Fig. 6C), suggesting that lowering triglyceride could reduce phosphatidylserine externalization, which is in line with our previous results showing that triglycerides promote eryptosis (Fig. 4F). However, the size of RBCs was unaffected by both pharmacological interventions (Fig. 6D), suggesting that the release of premature RBCs and thereby anemic stress is unaffected by the treatment. Accordingly, the development of anemia could not be blunted by fenofibrate nor GW501516 treatment (Fig. 6E), indicating that eryptosis only contributes to a small extent to RBC elimination in the tumor context and that other factors account for the unfavorable RBC environment or activation of phagocytes. In contrast to the pharmacological approach, not only was phosphatidylserine externalization considerably lower in exercising TB mice (TB-ex) but also the increase in RBC size was normalized (Fig. 6, C and D). This effect likely resulted in a longer RBC survival and thereby attenuated development of anemia (Fig. 6E). Together, our data suggest that a targeted lowering of triglyceride levels is not sufficient to improve RBC life span, but that other factors that are affected by exercise are essential for RBC survival and thereby important to slow down the development of anemia.

Exercise might ameliorate tumor-associated anemia by reducing blood lactate and IL-1β

As exercise does not only normalize the lipid profile in blood but also elicits a variety of systemic effects such as an anti-inflammatory response, we assessed IL-1β levels in the plasma. The significant elevation of IL-1β in TB mice was blunted by the training intervention (Fig. 7A). Similarly, exercise could also prevent the rise in blood lactate in rest and after exercise (Fig. 7B), most likely due to a substantial elevation of the lactate importer monocarboxylate transporter 1 (MCT1; encoded by *Slc16a1*) and lactate dehydrogenase B (*Ldhb*), converting lactate to pyruvate, in skeletal muscle (Fig. 7C and fig. S5A). Exercise also elicited effects on tumor lactate handling (fig. S5A). For example, tumors of TB-ex mice could contribute to the lower blood lactate levels, as these tumors express higher levels of the lactate importer MCT1 and lower levels of the exporter

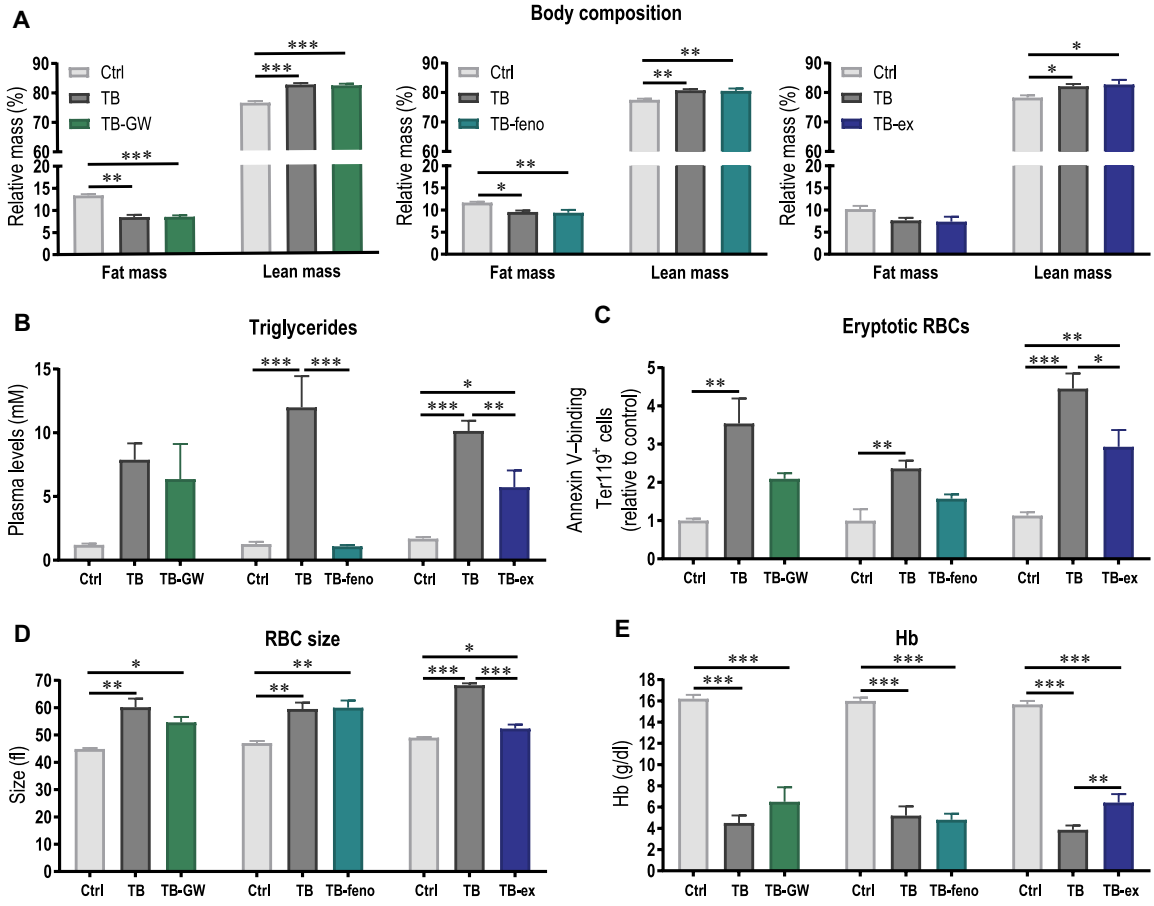

Fig. 6. Exercise ameliorates cancer-related anemia. To normalize lipid profile, fatty acid oxidation was increased in muscle or liver pharmacologically by treating mice with PPARδ agonist GW501516 (GW) or PPARα agonist fenofibrate (feno), respectively, or physiologically by exercise (ex). (**A**) Body composition of Ctrl, TB, and TB mice of pharmacological or physiological intervention groups was assessed by EchoMRI at the end of the intervention. (**B**) Triglyceride levels were measured in plasma. (**C**) As a measure for eryptosis, phosphatidylserine externalization in Ter119$^+$ RBCs was determined by annexin V binding using flow cytometry. (**D**) RBC size was assessed during blood count. (**E**) Hb levels were measured 3.5 weeks after tumor initiation. Differences between groups ($n = 5$ to 7 per group) were tested with one-way analyses of variance (ANOVAs) followed by Tukey's post hoc analysis, and data are represented as means + SEM. *$P < 0.05$, **$P < 0.01$, and ***$P < 0.001$.

MCT4 (encoded by *Slc16a3*). However, despite the reduction in circulating IL-1β in TB-ex animals, only minimal changes in the expression of a selection of cytokines and chemokines were found in the liver and tumor of TB and TB-ex animals (fig. S5, B and C).

As we have observed that IL-1β but not lactate promotes phosphatidylserine externalization on RBCs and thereby could contribute to reduced RBC survival, we next studied whether IL-1β or lactate could directly affect the phagocytic activity of splenocytes. First, we FACS (fluorescence-activated cell sorting)–sorted these phagocytes and measured gene expression to assess whether splenic phagocytes express lactate transporters and IL1R1 (Fig. 7D). The lactate importer MCT1 and exporter MCT4 are expressed by these cells, and, in TB mice, mRNA levels of both transporters are substantially elevated compared to Ctrl (Fig. 7D). In addition, these cells also express *Il1r1*, suggesting that lactate and IL-1β could affect cellular activity. Notably, phagocytes of TB mice express high levels of IL-1β, which could contribute to the observed inflammatory profile and affect RBC survival (Fig. 7D). To investigate whether the normalization of IL-1β and lactate levels could affect RBC survival, we tested the effects of IL-1β and lactate on erythrophagocytosis in vitro. Splenocytes and PKH26-labeled RBCs of healthy Ctrl mice were treated with pathophysiological levels of IL-1β, lactate, or medium only (untreated) for 1 hour. Subsequently, the cells were washed and pretreated, and untreated splenocytes were coincubated with untreated or pretreated RBCs, respectively. In the Ctrl condition, untreated splenocytes were coincubated with untreated RBCs. While pretreating RBC did not affect their susceptibility to be phagocytosed, pretreating splenocytes with either IL-1β or lactate lead to a higher number of highly PKH26-fluorescent F4/80^{high}CD11b^{high} and F4/80^{low}CD11b^{high} cells that show internalization of entire RBCs (Fig. 7E and fig. S6). Our data therefore suggest that IL-1β and lactate increase the phagocytic activity of splenocytes to engulf healthy RBCs. Thus, exercise might ameliorate RBC life span by preventing the tumor-induced elevation in IL-1β and lactate level.

In line with the assumption of the partially preserved RBC life span, the spleen size of TB-ex mice was considerably smaller compared to that of TB mice (Fig. 8A). To verify whether these exercised mice experience less anemic stress, *Epo* expression in kidney and EPO plasma levels were determined (Fig. 8B). In line with the higher Hb levels in TB-ex mice (Fig. 6E), *Epo* expression in the kidney was lower compared to that of TB mice, which was substantially (~300-fold) elevated compared to Ctrl animals. Although

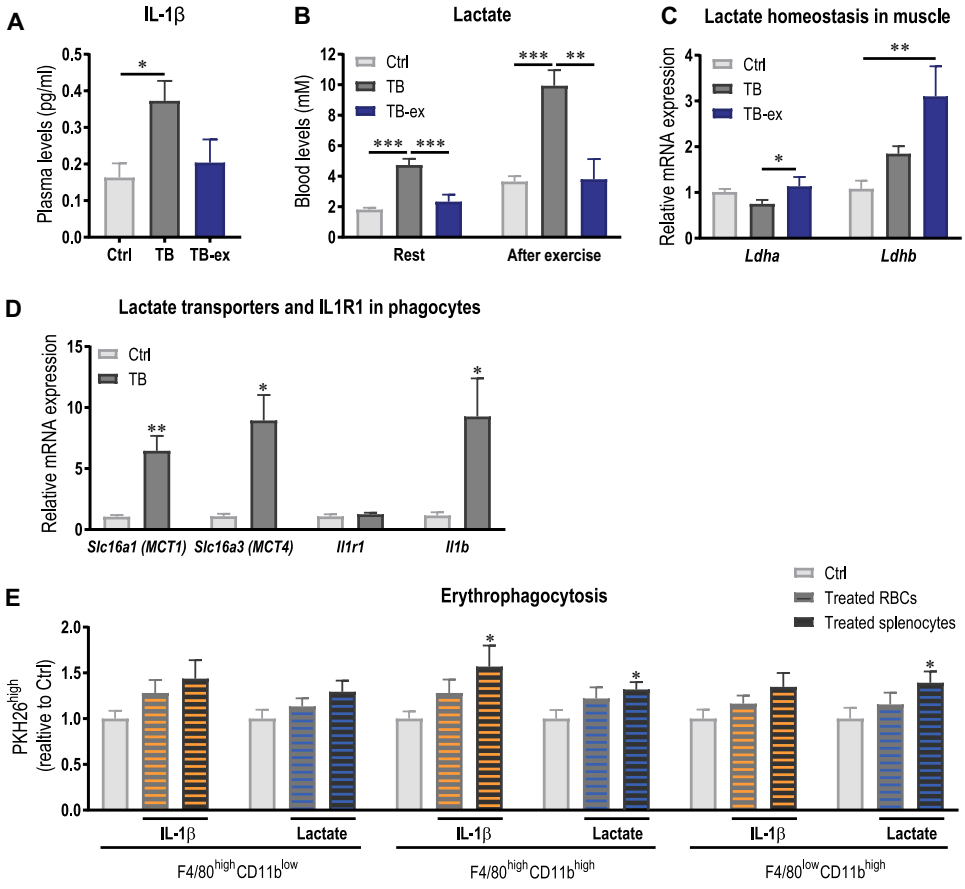

Fig. 7. Exercise ameliorates anemia by its anti-inflammatory effects and the normalization of the metabolic profile. (**A**) IL-1β levels were assessed in plasma of Ctrl, TB, and TB-ex 3.5 weeks after tumor initiation. (**B**) Blood lactate levels in rest and immediately after exhausting exercise. (**C**) Relative mRNA expression levels of *Ldha* and *Ldhb* that convert pyruvate to lactate or lactate to pyruvate, respectively, were measured in muscle. (**D**) To assess the expression of lactate transporters MCT1 and MCT4 and *Il1r1*, splenic phagocytes were FACS-sorted and mRNA levels were determined by qPCR. Expression of *Il1b* was also determined. (**E**) PKH26 fluorescently labeled healthy RBCs and healthy splenocytes were preincubated separately with pathophysiological levels of IL-1β (1 pg/ml) or lactate (10 mM) and then coincubated with either untreated splenocytes or untreated RBCs. These conditions were compared to the Ctrl condition in which untreated splenocytes were coincubated with untreated RBCs. Quantification of the percentage PKH26^{high} cells that engulfed complete RBCs is shown. Differences between groups ($n = 5$ to 7 per group) were tested with one-way ANOVAs followed by Tukey's post hoc analysis, and data are represented as means + SEM. Data of in vitro erythrophagocytosis experiments consist of three independent experiments with three to four biological replicates, and Ctrl and treatment groups were compared by two-tailed unpaired *t* tests with Welch's correction. If not indicated otherwise by a line, then asterisks indicate differences between Ctrl and treated group. *$P < 0.05$, **$P < 0.01$, and ***$P < 0.001$. Slc16a, solute carrier family 16 member.

EPO levels in plasma were increased in TB and TB-ex mice, levels in TB-ex animals were considerably reduced, suggesting that the overall anemic stress was decreased in the TB-ex group. Notably, the accumulation of stage IV RBCs was rescued by exercise (Fig. 8C), which is also in line with the normalized RBC size (Fig. 6D) and demonstrating the positive effects on RBC environment, maturation, and survival. Furthermore, in addition to the amelioration of anemia 3.5 weeks after LLC inoculation, exercise delayed the onset of anemia (Fig. 8D). Last, we investigated whether these alterations resulted in enhanced physical performance. TB-ex mice were not only able to run longer than TB animals but there was also even a considerable elevation in endurance performance compared to healthy, untrained Ctrl mice (Fig. 8E). Collectively, our data reveal that exercise ameliorates the development of tumor-associated anemia by preserving a favorable environment for RBCs and thereby promoting RBC survival. This results in a substantial improvement in physical performance that can have meaningful implications for patients with cancer suffering from anemia and fatigue.

DISCUSSION

A high number of patients with cancer suffer from anemia, with devastating effects on quality of life and survival, aggravated by a lack of efficacious, safe, and targeted therapeutic options. Therefore, a better understanding of the underlying mechanisms of tumor-associated anemia is fundamental to develop novel treatment strategies. In this study, we demonstrate that reduced RBC survival substantially contributes to the development of anemia. We provide solid evidence that the tumor-induced immune response and metabolic remodeling result in an unfavorable environment for RBCs leading to premature elimination. We show that exercise is able to partially normalize the systemic metabolic and immune profiles of TB mice and thereby ameliorates anemia and improves fatigability and endurance (Fig. 9). Thus, in cancer patients with pretreatment anemia, individuals in-between bouts of chemotherapy or bone marrow radiotherapy, or patients treated with immunotherapy or non–bone marrow radiotherapy, exercise, or interventions leveraging exercise-like effects, has a high potential to alleviate anemia by

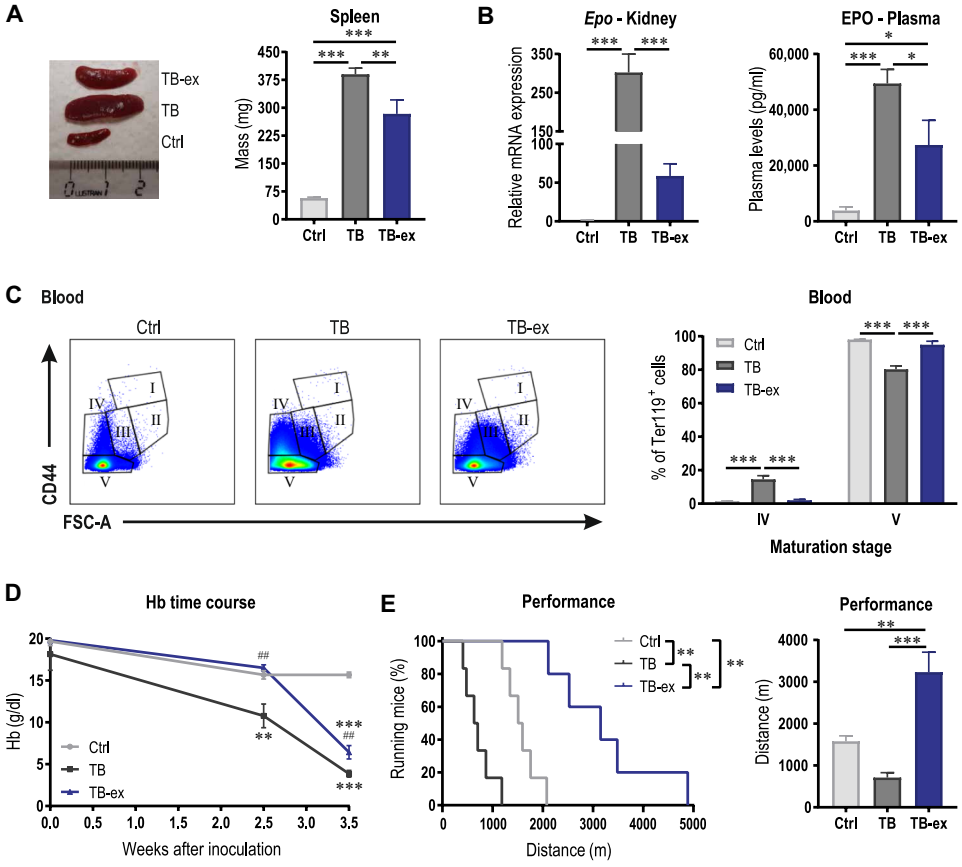

Fig. 8. Exercise delays the onset of anemia and substantially elevates performance. (**A**) Representative image and quantified spleen mass of Ctrl, TB, and TB-ex mice 3.5 weeks after tumor cell inoculation. The ruler is in centimeters. (**B**) EPO levels in kidney and plasma. (**C**) Maturation of Ter119$^+$ cells in blood were analyzed according to their size and CD44 expression as shown in the representative flow cytometry plots and quantified in the bar graph. (**D**) Time course of Hb levels in Ctrl, TB, and TB-ex mice throughout the study. (**E**) The effects of the intervention on maximal performance tested on a motorized treadmill represented as a Kaplan-Meier Curve or bar graph showing maximal distance covered by the mice. Kaplan-Meier curves were compared with a log-rank test, differences between groups ($n = 5$ to 7 per group) were tested with one-way ANOVAs followed by Tukey's post hoc analysis, and data are represented as means + SEM. *$P < 0.05$, **$P < 0.01$, and ***$P < 0.001$. In (D), asterisks indicate differences compared to Ctrl mice and # compared to TB mice. Photo credit: Regula Furrer, University of Basel.

mitigating RBC destruction, thereby complementing EPO-based standard therapy for treatment-caused anemia that boosts erythropoiesis. Notably, patients suffering from different degrees of anemia, even only mild forms, might profit from these therapies, as also mild anemia can lead to fatigue and reduced quality of life (*34*).

Even in the absence of metastases, primary tumors elicit a massive, multifactorial remodeling of systemic immune function and metabolic profiles (*35*). For example, our metabolomics interrogation revealed a comprehensive alteration in circulating lipids, closely correlated to tumor-induced lipolysis in adipose tissue and a reduction in fatty acid oxidation in the liver. Intriguingly, we identified individual metabolites and cytokines—e.g., specific triglyceride species, lactate, or IL-1β—that affect RBC levels by modulating eryptosis or phagocytosis. These and other metabolites and cytokines most likely synergize, potentially with reactive oxygen species and other compounds, to collectively reduce RBC levels and trigger tumor-associated anemia (*11*, *22*, *24*, *36*). The complexity of these interactions was underlined by the inability of narrow pharmacological interventions to rectify this pathological process, e.g., those aimed at lowering circulating triglycerides by activating PPARα or PPARδ. These experiments furthermore revealed that mitigation of eryptosis in the absence of additional benefits on erythrophagocytosis is insufficient to elevate Hb in cancer. In stark contrast, endurance training, which elicits multifactorial and multisystemic effects, was much more potent in reducing anemia and boosting endurance in TB animals.

Current therapies for cancer-related anemia aim at increasing RBC production, which is most notably impaired in treatment-induced anemia (*7*). We now provide strong evidence in our primary tumor model—where tumor anemia develops in parallel to tumor growth—that the systemic physiological anemia response is preserved as reflected by the dynamic EPO regulation and production and the ensuing erythropoietic process. EPO production is highly elevated in TB mice and associated with extramedullary erythropoiesis. The incomplete maturation and premature release of RBC precursors would indicate that a further acceleration of erythropoiesis by pharmacological means could be detrimental. Furthermore, as a reserve erythropoietic organ, we and others show a remarkable increase in spleen size that is mainly attributed to the augmentation in erythroid Ter119$^+$ cells, while the proportion B cells and T cells decrease with tumor progression (*27*, *37*). These Ter119$^+$ cells in the spleen of TB mice not only contribute to the stress-induced erythropoiesis

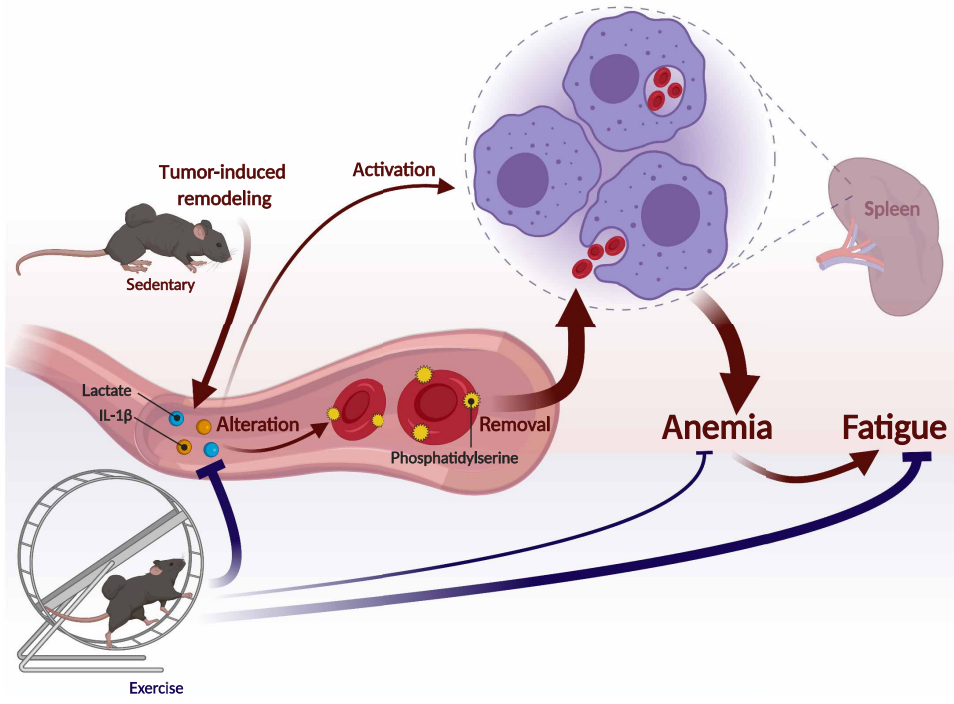

Fig. 9. Exercise mitigates tumor-associated anemia. Graphical illustration of tumor-induced inflammatory and metabolic remodeling that affects RBC survival by activating splenic phagocytes and increasing the susceptibility of RBCs to be eliminated, which eventually results in anemia and increased fatiguability. Exercise can partially normalize this tumor-induced remodeling and thereby ameliorate the development of anemia and substantially elevate performance. This figure was created with BioRender.com.

but also secrete factors that are associated with tumor progression and reduced survival (*37*). Therefore, instead of targeting production, tumor anemia therapies should blunt the elevated destruction of RBCs on several levels.

Our findings point toward a change in the RBC environment leading to intrinsic alterations that trigger eryptosis and consequently removal. To maintain RBC integrity, hepatic and splenic phagocytes rapidly eliminate stressed RBCs (*30*, *38*). In addition, tumor-induced systemic changes also alter the activation state of splenic macrophages, e.g., as indicated by the greater propensity of such macrophages to phagocytose RBCs derived from healthy animals. Collectively, the systemic environment evoked by the tumor thus results in compromised RBCs marked for removal and activation of macrophages to engulf RBCs even in the absence of stress markers including externalized phosphatidylserine and abnormal mean corpuscular volume (MCV). In light of the minor effect of mitigating eryptosis, MCV might be a more relevant and accessible parameter to determine therapeutic efficacy in tumor-associated anemia than phosphatidylserine. High MCV predicts poor overall survival of patients with cancer (*39*, *40*), which further highlights the therapeutic potential of exercise to enhance survival.

We now describe lactate and IL-1β as two examples of circulating factors that are altered in TB mice and that affect RBC and macrophage behavior. A normalization of the levels of these and other systemic metabolites, cytokines, and hormones could therefore be leveraged to clinically address cancer anemia in patients. For example, several IL-1β inhibitors are already Food and Drug Administration–approved (*41*), and treating participants with a history of myocardial infarction with the monoclonal anti–IL-1β antibody canakinumab reduced the incidence of anemia during the 5-year study period (*42*). Although a phase 1 clinical trial treating breast cancer patients with the IL-1β receptor antagonist anakinra has been conducted (NCT01802970), results on anemia have not been published so far. Therefore, it is still ill-defined whether blocking IL-1β in patients with cancer ameliorates anemia. Until efficacious and safe pharmacological interventions are found, exercise-based approaches could provide significant relief of anemia and the ensuing pathologies. In our studies, endurance training normalized metabolic parameters and inflammation in TB animals and elevated Hb levels. Moreover, exercised animals exhibited several hallmarks of reduced anemic stress, including lower EPO production and premature release of RBCs progenitors and a blunted splenomegaly and thus extramedullary erythropoiesis. This normalization in spleen size also lowers the abundance of $F4/80^{high}CD11b^{low}$ RPMs and $F4/80^{high}CD11b^{high}$ macrophages and thereby suppresses the total erythrophagocytic potential of the spleen. A limitation of this study is, however, that this was so far only shown in one tumor model, and it would be important to replicate these finding with other types of tumors. In addition, the dissection of exercise-induced benefits in a metastatic tumor model and an experimental group receiving treatment would further improve our understanding on the exercise effects on cancer-related anemia in general. Last, the translational implementation of such interventions to patients in the clinic will also be subject for future research.

Notably, the substantial increase in performance in TB-ex mice highlights the importance of physical activity in the treatment of fatigue that could have a major impact on quality of life. The multifactorial effects of exercise can be essential in the treatment of patients with cancer regarding quality of life, cancer recurrence, and survival (*43*–*45*). Even during ongoing cancer-reductive therapy, exercise

could significantly improve physical functionality and fatigue and reduce treatment-induced adverse effects that all contributed to increase quality of life (*46*, *47*). In preclinical models, exercise could even elevate chemotherapy efficacy (*48*). However, the experienced fatigue, the time-consuming therapies and nausea, physical impairments, a catabolic state, and low-energy substrate levels often impede the engagement in exercise training in patients with cancer. Training interventions thus have to be guided, supervised, and individually adjusted to comorbidities and symptoms (*49*). Furthermore, it is instrumental to understand the underlying systemic, cellular, and molecular mechanisms to design treatments that could promote exercise effects and/or facilitate exercise-based therapies. Nevertheless, if patients are able to perform exercise, then endurance training is a potent, safe, and cost-effective therapeutic intervention to alleviate cancer-related symptoms such as reduced physical functionality and fatigue and possibly tumor-associated anemia. This could improve quality of life and could thereby have a major impact for patients with cancer.

MATERIALS AND METHODS

Experimental design

For this study, male C57BL/6J mice were kept under standard conditions with a 12-hour light/12-hour dark cycle and food and water ad libitum. To study the effects of the tumor and interventions on anemia, we used a randomized study design. At the age of 16 to 18 weeks, tumor cells were injected into the flank of the mice and 25 days (3.5 weeks) after tumor cell inoculation, mice were sacrificed. One of the pharmacological interventions (GW501516) started concomitant with tumor injection, while treatment with fenofibrate started 10 days after injection. The exercise intervention started 4 weeks before tumor cell inoculation. To exclude any acute effects of the intervention, mice assigned to pharmacological or exercise intervention were sacrificed 24 or 48 hours after the last injection or exercise bout, respectively. On the last day, body composition of the mice was assessed with an EchoMRI (Medical Systems). During the dissection, blood was collected from the vena cava in Li-heparin– and EDTA-coated tubes (Sarstedt), and plasma was stored for further analysis. Furthermore, tumor, spleen, and different WAT depots were removed and weighted. In addition, bone marrow, spleen, kidney, liver, and muscle tissues were collected and either immediately processed and analyzed by flow cytometry or frozen in liquid nitrogen for later analyses. All experiments were approved by the Kantonales Veterinäramt Basel-Stadt and followed the Swiss guidelines for animal experimentation and care.

Tumor model

To study tumor-associated anemia, we chose a well-established primary tumor model that is known to develop robust anemia (*50*) and that is unlikely to metastasize within the 3.5-week study period. In addition, anemia induced by tumors originating from LLC show characteristics observed in anemic patients with cancer (*27*). To induce tumors, LLC cells were subcutaneously injected into the flank. LLC cells obtained from the American Type Culture Collection (ATCC CRL-1642) were first proliferated for 5 days in Dulbecco's modified Eagle's medium (DMEM) containing 10% fetal bovine serum (FBS). Then, cells were resuspended in phosphate-buffered saline (PBS) at a concentration of 1×10^6 cells/ml of which 100 µl was injected (1×10^5 cells). Ctrl animals were injected with 100 µl of PBS. During this procedure, mice were anesthetized using inhalation anesthesia. Mice that did not develop a palpable tumor after 2 weeks usually never developed a tumor and were therefore excluded from the study ($n = 3$). Postmortem, mice were analyzed for the occurrence of metastases.

Pharmacological intervention

During the pharmacological intervention, aimed at increasing fatty acid oxidation in muscle or liver, mice were intraperitoneally injected with the PPARδ agonist GW501516 (AdipoGen Life Sciences) or the PPARα agonist fenofibrate (Sigma-Aldrich). GW501516 was dissolved in 2.5% dimethyl sulfoxide (DMSO) and saline and injected with a final concentration of 5 mg/kg body weight (injection volume was 5 µl/g body weight). Fenofibrate was dissolved in corn oil (Sigma-Aldrich), and a final concentration of 50 mg/kg body weight in a total volume of 50 µl was injected. Ctrl mice received vehicle injections of either 2.5% DMSO in saline or 50 µl of corn oil.

Exercise intervention

To maximize the time and effects of the exercise intervention and to prime the immune system as shown previously (*46*), TB mice subjected to the exercise intervention group (TB-ex) received running wheels (Columbus Instruments) 4 weeks before tumor initiation. Mice had free-running wheel access until 48 hours before the termination of the experiment, and voluntary running activity was recorded throughout the experimental period. In addition to free-running wheel access, mice were trained on a motor-driven treadmill (Columbus Instruments) 5 days/week for 1 hour. The training started 3 weeks before LLC injection, and the last training was performed 48 hours before the termination of the experiment. The training was performed at an inclination of 5°, and the velocity was progressively increased up to 2 weeks after inoculation (to 20 m/min) and was thereafter slightly reduced because of disease progression. Mice that did not run on the treadmill and covered less than 1 km/day in the running wheels were excluded from the study. Maximal performance was tested half a week before the end of the experiment. Mice that have not ran on a treadmill before were acclimatized to treadmill running for 2 days. The maximal performance test was executed at an inclination of 5° and started with 5 min at 5 m/min, followed by 5 min at 8 m/min and 15 min at 10 m/min. Subsequently, velocity was increased every 15 min by 2 m/min until exhaustion. Exhaustion was defined as the time point at which mice could not further keep up with the speed. An electrical grid at the end of the treadmill was used as motivational stimulus.

Longitudinal blood measurements

Hb levels were assessed by performing a blood count (ADVIA 2120, Siemens) or using a Hb analyzer (EKF Diagnostics). Blood lactate was measured with a lactate meter (Nova Biomedical). To trace RBCs and thereby assess RBC life span, EZ-Link Sulfo-NHS-Biotin (100 mg/kg body weight; Thermo Fisher Scientific) was intravenously injected 3 days before tumor cell inoculation (*51*). Every 3 to 7 days, 2 µl of blood were stained with Ter119-phycoerythrin (PE) (1:200; clone TER-119, BioLegend) and streptavidin-allophycocyanin (APC) (1:200; BioLegend) and analyzed on BD FACSCanto II.

Plasma analysis

Cytokine levels of TNFα and IL-1β were measured in plasma using the customized V-PLEX Proinflammatory Panel 1 Mouse Kit (Meso

Scale Discovery). Free fatty acids in plasma were assesses with the Free Fatty Acid Quantitation Kit MAK044 (Sigma-Aldrich), triglycerides using the cobas c 111 analyzer (Roche Diagnostics AG), and EPO levels with the mouse EPO PicoKine ELISA Kit (Boster Biological Technology). All analyses were performed according to the manufacturers' protocols.

A global overview of acylcarnitine and triglyceride levels in plasma was obtained by targeted mass spectrometry–based metabolomics using the AbsoluteIDQ p400 HR Kit (Biocrates Life Sciences AG, Innsbruck, Austria) and performed by Biocrates according to the manufacturer's instructions as described previously (*52*). Data were analyzed with the Biocrates MetIDQ software.

Single-cell suspensions

Single-cell suspensions of the bone marrow and spleen were prepared immediately after the dissection. Cell suspension of the bone marrow was obtained by mechanical dissociation of the tibia using a mortar and subsequently filtering through a 70-μm cell strainer (Falcon). The spleen was mashed through a 70-μm cell strainer. To remove RBCs from the spleen cell suspension used for the erythrophagocytosis assay, RBCs were lysed in ACK lysing buffer (Gibco).

Erythrophagocytosis

For the erythrophagocytosis assay, blood was collected in EDTA-coated tubes and centrifuged for 10 min at 400*g*. After removing the buffy coat, RBCs were washed with PBS. To fluorescently label RBCs, the PKH26 Red Fluorescent Cell Linker Kit (Sigma-Aldrich) was used. Ten to fifty microliters of packed RBCs were resuspended in 100 to 500 μl of diluent C and 100 to 500 μl of diluent C containing 4 μM PKH26 dye and incubated for 5 min protected from light. The reaction was stopped by incubation with the equal volume of FBS for 1 min. RBCs were washed twice with PBS containing 5% FBS. To assess erythrophagocytosis, 4×10^6 splenocytes were mixed with 2.5 μl of packed PKH26-labeled RBCs and coincubated in DMEM containing 10% FBS for 1 hour at 37°C in a humidified 5% CO_2 incubator. After 1 hour, remaining RBCs were removed using ACK lysing buffer. Following this, cells were prepared for flow cytometry (see below).

In vitro experiments

To test the eryptotic potential of the identified candidates, blood was collected in Li-heparin–coated tubes and centrifuged for 20 min at 120*g* as previously described (*53*). Supernatant was discarded and RBCs were washed in Ringer solution containing 125 mM NaCl, 5 mM KCl, 1 mM $MgSO_4$, 32 mM N-2-hydroxyethylpiperazine-N-2-ethanesulfonic acid (Hepes), 5 mM glucose, and 1 mM $CaCl_2$ (pH 7.4). RBCs were incubated in Ringer solution containing recombinant mouse IL-1β (1 pg/ml; BioLegend), 10 mM sodium L-lactate (Sigma-Aldrich), 2 μM propionylcarnitine (Sigma-Aldrich), 1 μM valerylcarnitine (MedChemExpress), 600 μM TG(54:4) (Sigma-Aldrich), or vehicle Ctrl at a hematocrit of 0.4% for 24 hours at 37°C in a humidified 5% CO_2 incubator. After 24 hours, RBCs were washed and stained with annexin V–fluorescein isothiocyanate (FITC; 1:100; BioLegend) and measured on BD FACSCanto II as described below.

To investigate the effects of IL-1β and lactate on erythrophagocytosis, splenocytes of healthy Ctrl mice were isolated and RBCs were labeled with PKH26 as described in the previous sections. Splenocytes and labeled RBCs were preincubated in DMEM containing 10% FBS alone or with additional recombinant mouse IL-1β (1 pg/ml) or sodium L-lactate (10 mM) for 1 hour. After 1 hour, cells were washed and 4×10^6 pretreated splenocytes were coincubated with 2.5 μl of untreated RBCs and 4×10^6 untreated splenocytes with 2.5 μl of pretreated and untreated RBCs. After incubating for 1 hour, remaining RBCs were lysed using ACK lysing buffer and prepared for flow cytometry or FACS sorting as describe below.

Flow cytometry

To assess RBC maturation (*54*, *55*), bone marrow and spleen cells were treated with TruStain FcX (1:200; clone 93, BioLegend) and stained in PBS containing 5% FBS using the following antibodies: CD71-FITC (1:200; clone RI7217, BioLegend), Ter119-PE (1:200; clone TER-119, BioLegend), CD44-PE/Cy7 (1:400; clone IM7, BioLegend), and SYTOX Blue dead cell stain (1:5000; Invitrogen). Blood was first stained with Ter119-PE and CD44-PE/Cy7 and subsequently with annexin V–FITC (1:100; BioLegend) using annexin V binding buffer (BioLegend) to assess phosphatidylserine externalization. Cells were analyzed on BD FACSCanto II. To analyze DNA content in RBC, blood was first stained in PBS containing 5% FBS with CD71-FITC (1:200; clone RI7217, BioLegend), Ter119-PE (1:200; clone TER-119, BioLegend), and subsequently with DRAQ5 (1:1000; BioLegend). Cells were analyzed on BD LSRFortessa. Splenocytes from the erythrophagocytosis assays were treated with TruStain FcX (1:200) and stained in PBS containing 5% FBS using the following antibodies: CD45-APC/Cy7 (1:200; clone 30-F11, BioLegend), CD11b-FITC (1:200; clone M1/70, BioLegend), F4/80-APC (1:100; clone BM8, BioLegend), and SYTOX Blue dead cell stain (1:5000; Invitrogen). Cells were analyzed on BD LSRFortessa (a subset was measured on ImageStreamX® Mark II as described below). To determine the composition of the spleen, splenocytes (both prior and after performing RBC lysis) were treated with TruStain FcX (1:200; clone 93, BioLegend) and stained in PBS containing 5% FBS using the following antibodies: CD45-APC/Cy7 (1:200; clone 30-F11, BioLegend), CD71-FITC (1:200; clone RI7217, BioLegend), Ter119-PE (1:200; clone TER-119, BioLegend), and SYTOX Blue dead cell stain (1:5000; Invitrogen). Cells were analyzed on BD LSRFortessa. For the assessment of the $CD45^+$ population in the spleen, splenocytes were treated with TruStain FcX (1:200; clone 93, BioLegend) and stained in PBS using the following antibodies: CD11b-FITC (1:100: clone M1/70, BioLegend), B220-BV421 (1:100; clone RA3-6B2; BioLegend), CD4-BV510 (1:100; clone RM4-5, BioLegend), CD19-BV605 (1:100; clone 6D5, BioLegend), CD3-BV711 (1:100; clone 17A2, BioLegend), CD8-BV785 (1:100; clone 53-6.7, BioLegend), F4/80-PE (1:100; clone BM8, BioLegend), CD11c-PE/Cy7 (1:100; clone N418, BioLegend), NK1.1-APC (1:80; clone PK136, BioLegend), CD45-AF700 (1:200; clone 30-F11, BioLegend), and viability-APC/Cy7 (1:2000; Invitrogen). Cells were analyzed on BD LSRFortessa. Data analysis was performed using the FlowJo V10 software.

FACS sorting

Cell suspension of splenocytes was treated with TruStain FcX (1:200; clone 93, BioLegend) and stained in PBS containing 5% FBS using the following antibodies: CD45-APC/Cy7 (1:200; clone 30-F11, BioLegend), CD11b-PE/Cy7 (1:100; clone M1/70, BioLegend), BV605-F4/80 (1:100; clone BM8, BioLegend), and SYTOX Blue dead cell stain (1:5000; Invitrogen). Phagocytes were sorted on BD FACSAria Fusion.

Imaging flow cytometry

Samples were prepared as described for the other erythrophagocytosis experiments (see the "In vitro experiments" and "Flow cytometry" sections). All samples were acquired using a 12-channel Amnis® brand ImageStreamX® Mark II (Luminex, Austin, Texas) imaging flow cytometer equipped with four excitation lasers [120 mW (405 nm), 200 mW (488 nm), 200 mW (561 nm), and 150 mW (642 nm)] and a MultiMag with three objectives lenses (×20, ×40, and ×60 magnification). Samples were acquired at ×60 magnification, and the excitation lasers (405, 488, and 642 nm) were used at full power. Single-color compensation controls for CD11b-FITC, PKH26, SYTOX Blue dead cell stain-PB, F4/80-APC, and CD45-APC/Cy7 were also acquired using the integrated software INSPIRE® (Luminex) for data collection.

Image analysis was performed using image-based algorithms in the ImageStream Data Exploration and Analysis Software (IDEAS® 6.2.187, Luminex). Typical files contained imagery for 50,000 to 100,000 cells. The analysis was restricted to single cells in best focus. Single cells were identified by their intermediate size (area) and high aspect ratio (minor axis divided by the major axis) in comparison to debris (small area and a range of aspect ratios depending on the shape of the debris) and doublets (large area and small aspect ratio). Out-of-focus events were excluded by using the feature bright-field gradient RMS, a measurement of image contrast. Only living cells negative for the LIVE/DEAD marker were selected to quantify the internalization of erythrocytes. To calculate the internalization, a mask was designed that identifies the inside of the cells. The tight object mask of the CD45 image was used to define the area corresponding to the cell. This mask was eroded by 2 pixels to exclude the cell membrane. The intracellular mask was then used to calculate the Internalization feature applied to the PKH26 channel. Internalization is defined as the ratio of the PKH26 intensity inside the cell (the intracellular mask) to the intensity of the entire cell. This ratio is log-transformed to increase the dynamic range (−inf to +inf). Internalized cells typically have positive scores, while cells with little internalization have negative scores.

To quantify the different RBC morphologies in the tumor and Ctrl samples, two super-features were generated using the Machine Learning (ML) module for IDEAS® 6.3. After manual selection of the "truth" populations, the ML algorithm calculates the super-feature that maximally separates each truth population from the others. This classifier is based on user-defined and/or ML-generated single features, which are ranked and combined by a Linear Discriminant Analysis. The two output classifiers (for stomatocyte-like and discocyte-like RBCs) contain a series of differentially weighted features targeted to the corresponding phenotype and are plotted in a two-dimensional scatter plot against each other. Events with values greater than zero are images that are best represented by the specific classifier. The analysis was restricted to $CD45^{-}PKH26^{+}$ singles cells.

RNA extraction and semi quantitative reverse transcription polymerase chain reaction analysis

Gene expression levels were determined in liver, kidney, spleen, and muscle tissues. Tissue was homogenized in 1 ml of TRIzol agent (Sigma-Aldrich) using FastPrep tubes (MP Biomedicals), and RNA was isolated according to the manufacturer's instructions. FACS-sorted phagocytes were pelleted by centrifugation for 5 min at 400*g* and disrupted in 350 µl of RLT buffer (Qiagen RNeasy Mini Kit) using a 30-gauge needle and syringe. RNA isolation was further performed according to the manufacturer's protocol. RNA concentration and quality were determined on the NanoDrop OneC spectrophotometer (Thermo Fisher Scientific). Subsequently, 1 µg of RNA was treated with deoxyribonuclease I (Invitrogen) and reverse-transcribed using the High Capacity cDNA RT Kit (Applied Biosystems). Because of limited material of FACS-sorted phagocytes, only 300 ng of RNA was reverse-transcribed using the High Capacity cDNA RT Kit (Applied Biosystems). Gene expression was measured on QuantStudio 5 Real-Time PCR System (Applied Biosystems) using Fast SYBR Green Master Mix (Applied Biosystems). Primer sequences are listed in Table 1. Values were normalized to the housekeeping gene [TATA box–binding protein (*Tbp*) or *18S*], and gene expression was expressed relative to the Ctrl group using the $2^{-\Delta\Delta Ct}$ method (or relative to the TB group in case of tumor tissue).

Protein isolation

To isolate proteins from RBCs, they were washed twice in PBS and centrifuged at 400*g* for 5 min followed by lysis in a 10-fold volume of ACK lysis buffer supplemented with protease and phosphatase inhibitor. Cellular debris was removed by centrifugation at 13,000*g* for 10 min, and protein concentration was determined in the supernatant using Bradford assay.

For proteins isolation from dissected pancreas, 30 mg of pancreas tissue was disrupted within protein lysis buffer (0.1% SDS, 1%NP-40, 5% glycerol, 1 mM EDTA, 150 mM NaCl, and 50 mM tris) using a tissue lyser. After 30-min incubation, lysate was centrifuged for at 13,000*g* for 10 min to remove tissue debris. Protein concentration was determined using Bradford assay.

Immunoprecipitation

For the detection of IL1RI in RBCs, 4000 µg of RBC protein was incubated for 16 hours with 1:100 diluted goat anti-mouse IL1RI antibody (no. AF771, R&D Systems) in 400 µl of protein lysis buffer under rotation. Subsequently, antibodies were captured by incubation with 50 µl of Protein A/G PLUS-Agarose (no. sc-2003, Santa Cruz Biotechnology) for 2 hours. Beads were washed consecutively with low-salt buffer [50 mM tris-HCl, 150 mM NaCl, 2 mM EDTA, and 1% Triton X-100 (pH 7.5)], high-salt buffer [50 mM tris-HCl, 500 mM NaCl, 2 mM EDTA, and 1% Triton X-100 (pH 7.5)], and LiCl wash buffer [50 tris-HCl, 250 mM LiCl, 2 mM EDTA, and 1% Triton X-100 (pH 7.5)] with centrifugation at 1000*g* for 30 s in between. Last, beads were incubated in 1× Laemmli buffer for 5 min at 95°C before Western blotting.

Western blotting

Protein lysates from RBCs were mixed with an equal volume of twofold protein lysis buffer (0.2% SDS, 2% NP-40, 10% glycerol, 2 mM EDTA, 300 mM NaCl, and 100 mM tris) before use. For Western blotting, 200 µg of RBC protein or 30 µg of pancreas protein was prepared with Laemmli buffer, incubated at 95°C for 5 min, and loaded onto a 15% polyacrylamide gel. Separated proteins were blotted onto membranes during 1 hour at 100 V. Subsequently, membranes were blocked against unspecific binding with 5% dry milk powder in TBS-T for 2 hours, followed by primary antibody incubation for 16 hours using either 1:500 diluted rabbit anti-mouse caspase 3 antibody (no. 9662, Cell Signaling Technology) or 1:1000 diluted goat anti-mouse IL1RI antibody (no. AF771, R&D Systems) in 1% bovine serum albumin (BSA)/TBS-T (Tris-buffered saline with 0.1% Tween-20). After three rounds of washing with TBS-T for

Table 1. Primer sequences used for qPCR analyses.

Gene	Forward (5′ to 3′)	Reverse (5′ to 3′)
Acadl	AGAAGTTCATCCCCCAGATGAC	GGCGTTCGTTCTTACTCCTTGT
Acadm	AACACTTACTATGCCTCGATTGCA	CCATAGCCTCCGAAAATCTGAA
Acads	CGGCAGAACAAGGGTATCAGT	TCCGGCAGTCCTCAAAGATG
Acadvl	ATGGGAGAAGCAGGCAAACA	CTCTGGGTGGACAATCCCTG
Alas2	TCCTGTCCAGTGCTCTCTCA	GGACAATGGCTCTTAGCCCA
Ccl2 (MCP-1)	TCTCCAGCCTACTCATTGGG	AGGTCCCTGTCATGCTTCTG
Ccl3 (MIP-1α)	TCCCAGCCAGGTGTCATTTT	TTGGAGTCAGCGCAGATCTG
CD36	GGCAAAGAACAGCAGCAAAAT	TGGCTAGATAACGAACTCTGTATGTGT
Clec2d	GGTTTGACAACCAGGATGAGC	TCTCCCCGGATGGGAATCG
Cox4i1	TACTTCGGTGTGCCTTCGA	TGACATGGGCCACATCAG
Cpt1a	ACTCCGCTCGCTCATTCCG	GATGCCATCAGGGGTGACTG
Cpt2	TACATCTCAGGCCCCTGGTTT	AACAGTCAAGTTGGTGGCCC
Cs	CCCAGGATACGGTCATGCA	GCAAACTCTCGCTGACAGGAA
Cycs	TGCCCAGTGCCACACTGT	CTGTCTTCCGCCCGAACA
Epo	CCACCCTGCTGCTTTTACTC	TGCACAACCCATCGTGACA
Epor	TAGGGCTGCATCATGGACAAA	TTCCTCCCAGAAACACACCA
Fam27f (*INAM*)	GGTGACCCTACTGACGGCT	CTCAGCGCATATCCCAGGA
Fech	GGTGAAGCTGCTGGATGAGTTA	GGACGTACCGGAATCCAATATAGTA
Gata1	CACCCTGAACTCGTCATACCA	GGCCCAGAGGAAAAGAAACCT
Il1b	GACGGACCCCAAAAGATGA	TGCTGCTGCGAGATTTGAAG
Il1R1	AGTAATGCTGTCCTGGGCTG	AGCACTTTCATATTCTCCATTTGTG
Il6	TAGTCCTTCCTACCCCAATTTCC	TTGGTCCTTAGCCACTCCTTC
Kitl (*SCF*)	TGCTGGTGCAATATGCTGGA	GTGATAATCCAAGTTTGTGTCTTCT
Ldha	GGATGAGCTTGCCCTTGTTG	TCCATCATCTCGCCCTTGA
Ldhb	TAAGATGGTGGTGGACAGTGC	GCATGGACTCGATGAGGTCAG
Sdhd	TTCTCTTAAAGCTGGGCGTTCT	GAAATGCTGACACATAAGCGGG
Tbp	TGCTGTTGGTGATTGTTGGT	CTGGCTTGTGTGGGAAAGAT
Slc16a1 (MCT1)	TACGCCGGAGTCTTTGGATT	TACCCGCGATGATGAGGATC
Slc16a3 (*MCT4*)	TCACGGGTTTCTCCTACGC	GCCAAAGCGGTTCACACAC
Tnf	ACGGCATGGATCTCAAAGAC	AGATAGCAAATCGGCTGACG
Tfrc	GTTTCTGCCAGCCCCTTATTAT	GCAAGGAAAGGATATGCAGCA
18S	AGTCCCTGCCCTTTGTACACA	CGATCCGAGGGCCTCACTA

10 min each, second antibody incubation using 1:10,000 dilutions of either swine anti-rabbit immunoglobulin G (IgG)/horseradish peroxidase (HRP) (no. P0399, Dako) or rabbit anti-goat IgG/HRP (no. P0449, Dako) in 1% BSA/TBS-T was performed. Protein bands were detected and visualized using SuperSignal West Femto substrate (no. 34094, Thermo Fisher Scientific) and a Vilber Fusion FX detector.

Statistical analyses

Statistical analyses were performed on GraphPad Prism 8. To exclude mice that showed an abnormal response to the tumor cell injection, a stringent outlier test ROUT (Q set at 0.1%) for Hb levels was performed that only detected definite outliers. Of the 41 TB mice, one had to be excluded. Differences between two groups were tested with two-tailed unpaired t tests with Welch's correction. One-way analyses of variance (ANOVAs) followed by Tukey's post hoc analysis were performed to test for differences between three groups. Kaplan-Meier curves were compared with a log-rank test. Differences with $P < 0.05$ were considered statistically significant. Values are presented as means + SEM, and n values are provided in the figure legend.

SUPPLEMENTARY MATERIALS

Supplementary material for this article is available at https://science.org/doi/10.1126/sciadv.abi4852

View/request a protocol for this paper from *Bio-protocol*.

REFERENCES AND NOTES

1. H. Ludwig, S. Van Belle, P. Barrett-Lee, G. Birgegard, C. Bokemeyer, P. Gascon, P. Kosmidis, M. Krzakowski, J. Nortier, P. Olmi, M. Schneider, D. Schrijvers, The European Cancer Anaemia Survey (ECAS): A large, multinational, prospective survey defining

the prevalence, incidence, and treatment of anaemia in cancer patients. *Eur. J. Cancer* **40**, 2293–2306 (2004).
2. C. Chen, Z. Song, W. Wang, J. Zhou, Baseline anemia and anemia grade are independent prognostic factors for stage IV non-small cell lung cancer. *Mol. Clin. Oncol.* **14**, 59 (2021).
3. Y. H. Zhang, Y. Lu, H. Lu, M. W. Zhang, Y. M. Zhou, X. L. Li, P. Lv, X. Y. Zhao, Pre-treatment hemoglobin levels are an independent prognostic factor in patients with non-small cell lung cancer. *Mol Clin Oncol* **9**, 44–49 (2018).
4. P. Kink, E. M. Egger, L. Lanser, M. Klaunzner, B. Holzner, W. Willenbacher, M. T. Kasseroler, D. Fuchs, G. Weiss, K. Kurz, Immune activation and anemia are associated with decreased quality of life in patients with solid tumors. *J. Clin. Med.* **9**, 3248 (2020).
5. R. Stasi, L. Abriani, P. Beccaglia, E. Terzoli, S. Amadori, Cancer-related fatigue: Evolving concepts in evaluation and treatment. *Cancer* **98**, 1786–1801 (2003).
6. J. J. Caro, M. Salas, A. Ward, G. Goss, Anemia as an independent prognostic factor for survival in patients with cancer: A systemic, quantitative review. *Cancer* **91**, 2214–2221 (2001).
7. G. Weiss, T. Ganz, L. T. Goodnough, Anemia of inflammation. *Blood* **133**, 40–50 (2019).
8. J. Bohlius, K. Schmidlin, C. Brillant, G. Schwarzer, S. Trelle, J. Seidenfeld, M. Zwahlen, M. Clarke, O. Weingart, S. Kluge, M. Piper, D. Rades, D. P. Steensma, B. Djulbegovic, M. F. Fey, I. Ray-Coquard, M. Machtay, V. Moebus, G. Thomas, M. Untch, M. Schumacher, M. Egger, A. Engert, Recombinant human erythropoiesis-stimulating agents and mortality in patients with cancer: A meta-analysis of randomised trials. *Lancet* **373**, 1532–1542 (2009).
9. K. K. Chan, K. B. Matchett, J. A. Coulter, H. F. Yuen, C. M. McCrudden, S. D. Zhang, G. W. Irwin, M. A. Davidson, T. Rulicke, S. Schober, L. Hengst, H. Jaekel, A. Platt-Higgins, P. S. Rudland, K. I. Mills, P. Maxwell, M. El-Tanani, T. R. Lappin, Erythropoietin drives breast cancer progression by activation of its receptor EPOR. *Oncotarget* **8**, 38251–38263 (2017).
10. J. L. Spivak, The anaemia of cancer: Death by a thousand cuts. *Nat. Rev. Cancer* **5**, 543–555 (2005).
11. A. Maccio, C. Madeddu, G. Gramignano, C. Mulas, L. Tanca, M. C. Cherchi, C. Floris, I. Omoto, A. Barracca, T. Ganz, The role of inflammation, iron, and nutritional status in cancer-related anemia: Results of a large, prospective, observational study. *Haematologica* **100**, 124–132 (2015).
12. M. Ozguroglu, B. Arun, G. Demir, F. Demirelli, N. M. Mandel, E. Buyukunal, S. Serdengecti, B. Berkarda, Serum erythropoietin level in anemic cancer patients. *Med. Oncol.* **17**, 29–34 (2000).
13. W. C. Faquin, T. J. Schneider, M. A. Goldberg, Effect of inflammatory cytokines on hypoxia-induced erythropoietin production. *Blood* **79**, 1987–1994 (1992).
14. M. U. Muckenthaler, S. Rivella, M. W. Hentze, B. Galy, A red carpet for iron metabolism. *Cell* **168**, 344–361 (2017).
15. M. L. Patchen, T. J. MacVittie, J. L. Williams, G. N. Schwartz, L. M. Souza, Administration of interleukin-6 stimulates multilineage hematopoiesis and accelerates recovery from radiation-induced hematopoietic depression. *Blood* **77**, 472–480 (1991).
16. C. S. Johnson, M. J. Chang, P. Furmanski, In vivo hematopoietic effects of tumor necrosis factor-alpha in normal and erythroleukemic mice: Characterization and therapeutic applications. *Blood* **72**, 1875–1883 (1988).
17. C. S. Johnson, D. J. Keckler, M. I. Topper, P. G. Braunschweiger, P. Furmanski, In vivo hematopoietic effects of recombinant interleukin-1 alpha in mice: Stimulation of granulocytic, monocytic, megakaryocytic, and early erythroid progenitors, suppression of late-stage erythropoiesis, and reversal of erythroid suppression with erythropoietin. *Blood* **73**, 678–683 (1989).
18. B. L. Mitlyng, J. A. Singh, J. K. Furne, J. Ruddy, M. D. Levitt, Use of breath carbon monoxide measurements to assess erythrocyte survival in subjects with chronic diseases. *Am. J. Hematol.* **81**, 432–438 (2006).
19. J. H. Li, J. F. Luo, Y. Jiang, Y. J. Ma, Y. Q. Ji, G. L. Zhu, C. Zhou, H. W. Chu, H. D. Zhang, Red blood cell lifespan shortening in patients with early-stage chronic kidney disease. *Kidney Blood Press. Res.* **44**, 1158–1165 (2019).
20. L. L. Moldawer, M. A. Marano, H. Wei, Y. Fong, M. L. Silen, G. Kuo, K. R. Manogue, H. Vlassara, H. Cohen, A. Cerami, S. F. Lowry, Cachectin/tumor necrosis factor-alpha alters red blood cell kinetics and induces anemia in vivo. *FASEB J.* **3**, 1637–1643 (1989).
21. S. M. Qadri, H. Mahmud, E. Lang, S. Gu, D. Bobbala, C. Zelenak, K. Jilani, A. Siegfried, M. Foller, F. Lang, Enhanced suicidal erythrocyte death in mice carrying a loss-of-function mutation of the adenomatous polyposis coli gene. *J. Cell. Mol. Med.* **16**, 1085–1093 (2012).
22. R. Bissinger, C. Schumacher, S. M. Qadri, S. Honisch, A. Malik, F. Gotz, H. G. Kopp, F. Lang, Enhanced eryptosis contributes to anemia in lung cancer patients. *Oncotarget* **7**, 14002–14014 (2016).
23. E. Pretorius, J. N. du Plooy, J. Bester, A comprehensive review on eryptosis. *Cell. Physiol. Biochem.* **39**, 1977–2000 (2016).
24. R. Bissinger, A. A. M. Bhuyan, S. M. Qadri, F. Lang, Oxidative stress, eryptosis and anemia: A pivotal mechanistic nexus in systemic diseases. *FEBS J.* **286**, 826–854 (2019).
25. T. Nemkov, S. M. Qadri, W. P. Sheffield, A. D'Alessandro, Decoding the metabolic landscape of pathophysiological stress-induced cell death in anucleate red blood cells. *Blood Transfus.* **18**, 130–142 (2020).
26. S. M. Qadri, R. Bissinger, Z. Solh, P. A. Oldenborg, Eryptosis in health and disease: A paradigm shift towards understanding the (patho)physiological implications of programmed cell death of erythrocytes. *Blood Rev.* **31**, 349–361 (2017).
27. L. Zhao, R. He, H. Long, B. Guo, Q. Jia, D. Qin, S. Q. Liu, Z. Wang, T. Xiang, J. Zhang, Y. Tan, J. Huang, J. Chen, F. Wang, M. Xiao, J. Gao, X. Yang, H. Zeng, X. Wang, C. Hu, P. B. Alexander, A. L. J. Symonds, J. Yu, Y. Wan, Q. J. Li, L. Ye, B. Zhu, Late-stage tumors induce anemia and immunosuppressive extramedullary erythroid progenitor cells. *Nat. Med.* **24**, 1536–1544 (2018).
28. R. E. Mebius, G. Kraal, Structure and function of the spleen. *Nat. Rev. Immunol.* **5**, 606–616 (2005).
29. P. Burger, E. Kostova, E. Bloem, P. Hilarius-Stokman, A. B. Meijer, T. K. van den Berg, A. J. Verhoeven, D. de Korte, R. van Bruggen, Potassium leakage primes stored erythrocytes for phosphatidylserine exposure and shedding of pro-coagulant vesicles. *Br. J. Haematol.* **160**, 377–386 (2013).
30. S. M. Meinderts, P. A. Oldenborg, B. M. Beuger, T. R. L. Klei, J. Johansson, T. W. Kuijpers, T. Matozaki, E. J. Huisman, M. de Haas, T. K. van den Berg, R. van Bruggen, Human and murine splenic neutrophils are potent phagocytes of IgG-opsonized red blood cells. *Blood Adv.* **1**, 875–886 (2017).
31. C. Roussel, M. Dussiot, M. Marin, A. Morel, P. A. Ndour, J. Duez, C. Le Van Kim, O. Hermine, Y. Colin, P. A. Buffet, P. Amireault, Spherocytic shift of red blood cells during storage provides a quantitative whole cell-based marker of the storage lesion. *Transfusion* **57**, 1007–1018 (2017).
32. D. Mandal, P. K. Moitra, S. Saha, J. Basu, Caspase 3 regulates phosphatidylserine externalization and phagocytosis of oxidatively stressed erythrocytes. *FEBS Lett.* **513**, 184–188 (2002).
33. K. C. Fearon, D. J. Glass, D. C. Guttridge, Cancer cachexia: Mediators, signaling, and metabolic pathways. *Cell Metab.* **16**, 153–166 (2012).
34. L. H. Gerber, Cancer-related fatigue: Persistent, pervasive, and problematic. *Phys. Med. Rehabil. Clin. N. Am.* **28**, 65–88 (2017).
35. G. Fonseca, J. Farkas, E. Dora, S. von Haehling, M. Lainscak, Cancer cachexia and related metabolic dysfunction. *Int. J. Mol. Sci.* **21**, 2321 (2020).
36. C. E. Pinzon-Diaz, J. V. Calderon-Salinas, M. M. Rosas-Flores, G. Hernandez, A. Lopez-Betancourt, M. A. Quintanar-Escorza, Eryptosis and oxidative damage in hypertensive and dyslipidemic patients. *Mol. Cell. Biochem.* **440**, 105–113 (2018).
37. Y. Han, Q. Liu, J. Hou, Y. Gu, Y. Zhang, Z. Chen, J. Fan, W. Zhou, S. Qiu, Y. Zhang, T. Dong, N. Li, Z. Jiang, H. Zhu, Q. Zhang, Y. Ma, L. Zhang, Q. Wang, Y. Yu, N. Li, X. Cao, Tumor-induced generation of splenic erythroblast-like Ter-cells promotes tumor progression. *Cell* **173**, 634–648.e12 (2018).
38. I. Theurl, I. Hilgendorf, M. Nairz, P. Tymoszuk, D. Haschka, M. Asshoff, S. He, L. M. Gerhardt, T. A. Holderried, M. Seifert, S. Sopper, A. M. Fenn, A. Anzai, S. Rattik, C. McAlpine, M. Theurl, P. Wieghofer, Y. Iwamoto, G. F. Weber, N. K. Harder, B. G. Chousterman, T. L. Arvedson, M. McKee, F. Wang, O. M. Lutz, E. Rezoagli, J. L. Babitt, L. Berra, M. Prinz, M. Nahrendorf, G. Weiss, R. Weissleder, H. Y. Lin, F. K. Swirski, On-demand erythrocyte disposal and iron recycling requires transient macrophages in the liver. *Nat. Med.* **22**, 945–951 (2016).
39. G. Jomrich, M. Hollenstein, M. John, R. Ristl, M. Paireder, I. Kristo, R. Asari, S. F. Schoppmann, High mean corpuscular volume predicts poor outcome for patients with gastroesophageal adenocarcinoma. *Ann. Surg. Oncol.* **26**, 976–985 (2019).
40. K. J. Li, W. Y. Gu, X. F. Xia, P. Zhang, C. L. Zou, Z. H. Fei, High Mean corpuscular volume as a predictor of poor overall survival in patients with esophageal cancer receiving concurrent chemoradiotherapy. *Cancer Manag. Res.* **12**, 7467–7474 (2020).
41. L. Arranz, M. D. M. Arriero, A. Villatoro, Interleukin-1β as emerging therapeutic target in hematological malignancies and potentially in their complications. *Blood Rev.* **31**, 306–317 (2017).
42. M. Vallurupalli, J. G. MacFadyen, R. J. Glynn, T. Thuren, P. Libby, N. Berliner, P. M. Ridker, Effects of interleukin-1β inhibition on incident anemia: Exploratory analyses from a randomized trial. *Ann. Intern. Med.* **172**, 523–532 (2020).
43. S. Morishita, Y. Hamaue, T. Fukushima, T. Tanaka, J. B. Fu, J. Nakano, Effect of exercise on mortality and recurrence in patients with cancer: A systematic review and meta-analysis. *Integr. Cancer Ther.* **19**, 1534735420917462 (2020).
44. F. S. Falcetta, H. de Araujo Vianna Trasel, F. K. de Almeida, M. R. R. Falcetta, M. Falavigna, D. D. Rosa, Effects of physical exercise after treatment of early breast cancer: Systematic review and meta-analysis. *Breast Cancer Res. Treat.* **170**, 455–476 (2018).
45. M. Trepanier, E. M. Minnella, T. Paradis, R. Awasthi, P. Kaneva, K. Schwartzman, F. Carli, G. M. Fried, L. S. Feldman, L. Lee, Improved disease-free survival after prehabilitation for colorectal cancer surgery. *Ann. Surg.* **270**, 493–501 (2019).
46. L. Pedersen, M. Idorn, G. H. Olofsson, B. Lauenborg, I. Nookaew, R. H. Hansen, H. H. Johannesen, J. C. Becker, K. S. Pedersen, C. Dethlefsen, J. Nielsen, J. Gehl, B. K. Pedersen, P. Thor Straten, P. Hojman, Voluntary running suppresses tumor growth through epinephrine- and IL-6-dependent NK cell mobilization and redistribution. *Cell Metab.* **23**, 554–562 (2016).

47. H. van Waart, M. M. Stuiver, W. H. van Harten, E. Geleijn, J. M. Kieffer, L. M. Buffart, M. de Maaker-Berkhof, E. Boven, J. Schrama, M. M. Geenen, J. M. M. Terwogt, A. van Bochove, V. Lustig, S. M. van den Heiligenberg, C. H. Smorenburg, J. A. H.-v. Vreeswijk, G. S. Sonke, N. K. Aaronson, Effect of low-intensity physical activity and moderate- to high-intensity physical exercise during adjuvant chemotherapy on physical fitness, fatigue, and chemotherapy completion rates: Results of the PACES randomized clinical trial. *J. Clin. Oncol.* **33**, 1918–1927 (2015).
48. C. A. Florez Bedoya, A. C. F. Cardoso, N. Parker, A. Ngo-Huang, M. Q. Petzel, M. P. Kim, D. Fogelman, S. G. Romero, H. Wang, M. Park, M. H. G. Katz, K. L. Schadler, Exercise during preoperative therapy increases tumor vascularity in pancreatic tumor patients. *Sci. Rep.* **9**, 13966 (2019).
49. M. van der Leeden, R. J. Huijsmans, E. Geleijn, M. de Rooij, I. R. Konings, L. M. Buffart, J. Dekker, M. M. Stuiver, Tailoring exercise interventions to comorbidities and treatment-induced adverse effects in patients with early stage breast cancer undergoing chemotherapy: A framework to support clinical decisions. *Disabil. Rehabil.* **40**, 486–496 (2018).
50. A. Kim, S. Rivera, D. Shprung, D. Limbrick, V. Gabayan, E. Nemeth, T. Ganz, Mouse models of anemia of cancer. *PLOS ONE* **9**, e93283 (2014).
51. A. Chow, M. Huggins, J. Ahmed, D. Hashimoto, D. Lucas, Y. Kunisaki, S. Pinho, M. Leboeuf, C. Noizat, N. van Rooijen, M. Tanaka, Z. J. Zhao, A. Bergman, M. Merad, P. S. Frenette, CD169+ macrophages provide a niche promoting erythropoiesis under homeostasis and stress. *Nat. Med.* **19**, 429–436 (2013).
52. H. Carlsson, S. Abujrais, S. Herman, P. E. Khoonsari, T. Akerfeldt, A. Svenningsson, J. Burman, K. Kultima, Targeted metabolomics of CSF in healthy individuals and patients with secondary progressive multiple sclerosis using high-resolution mass spectrometry. *Metabolomics* **16**, 26 (2020).
53. M. Arnold, R. Bissinger, F. Lang, Mitoxantrone-induced suicidal erythrocyte death. *Cell. Physiol. Biochem.* **34**, 1756–1767 (2014).
54. K. Chen, J. Liu, S. Heck, J. A. Chasis, X. An, N. Mohandas, Resolving the distinct stages in erythroid differentiation based on dynamic changes in membrane protein expression during erythropoiesis. *Proc. Natl. Acad. Sci. U.S.A.* **106**, 17413–17418 (2009).
55. J. Liu, J. Zhang, Y. Ginzburg, H. Li, F. Xue, L. De Franceschi, J. A. Chasis, N. Mohandas, X. An, Quantitative analysis of murine terminal erythroid differentiation in vivo: Novel method to study normal and disordered erythropoiesis. *Blood* **121**, e43–e49 (2013).

Acknowledgments: We thank S. Stefanova and J. Bögli from the FACS Core Facility of the Biozentrum for assistance, the FACS FlowTeam from the Department of Biomedicine of the University of Basel, and all animal caretakers from the Biozentrum for help. Last, we would also like to thank M. Donath and group from the Department of Biomedicine of the University of Basel for providing blood of IL1R1 global knock-out mice and support with the IL-1β experiments. **Funding:** This work is supported by the Swiss National Science Foundation (to C.H.), Swiss Cancer Research grant KFS-3733-08-2015 (to C.H.), Swiss Society for Research on Muscle Diseases (SSEM) (to C.H.), European Research Council (ERC) Consolidator grant 616830-MUSCLE_NET (to C.H.), Novartis Stiftung für Medizinisch-Biologische Forschung (to C.H.), and University of Basel (to C.H.). **Author contributions:** Conceptualization: R.F. and C.H. Methodology: R.F., A.J.J., T.N.R., and C.H. Investigation: R.F., A.J.J., T.N.R., S.D., and S.A.S. Analysis and interpretation: R.F., A.J.J., T.N.R., P.R., and C.H. Resources: M.R., R.C.S., and C.H. Funding acquisition: C.H. Supervision: M.R., R.C.S., and C.H. Writing (original draft): R.F. and C.H. Writing (review and editing): A.J.J., T.N.R., M.R., and R.C.S. **Competing interests:** The authors declare that they have no competing interests. P.R. is an employee of Luminex Corporation that manufactures the Amnis ImageStreamX® Mark II imaging flow cytometer. **Data and materials availability:** All data needed to evaluate the conclusions in the paper are present in the paper and/or the Supplementary Materials.

Submitted 12 March 2021
Accepted 15 July 2021
Published 8 September 2021
10.1126/sciadv.abi4852

Citation: R. Furrer, A. J. Jauch, T. Nageswara Rao, S. Dilbaz, P. Rhein, S. A. Steurer, M. Recher, R. C. Skoda, C. Handschin, Remodeling of metabolism and inflammation by exercise ameliorates tumor-associated anemia. *Sci. Adv.* **7**, eabi4852 (2021).

ScienceAdvances

Remodeling of metabolism and inflammation by exercise ameliorates tumor-associated anemia

Regula FurrerAnnaïse J. JauchTata Nageswara RaoSedat DilbazPeter RheinStefan A. SteurerMike RecherRadek C. SkodaChristoph Handschin

Sci. Adv., 7 (37), eabi4852. • DOI: 10.1126/sciadv.abi4852

Science Advances (ISSN) is published by the American Association for the Advancement of Science. 1200 New York Avenue NW, Washington, DC 20005. The title *Science Advances* is a registered trademark of AAAS.